MicroRNA-486–dependent modulation of DOCK3/PTEN/AKT signaling pathways improves muscular dystrophy–associated symptoms

Matthew S. Alexander,[1,2] Juan Carlos Casar,[3] Norio Motohashi,[4] Natássia M. Vieira,[1,2] Iris Eisenberg,[5] Jamie L. Marshall,[1,2] Molly J. Gasperini,[1] Angela Lek,[1,2] Jennifer A. Myers,[1] Elicia A. Estrella,[1,6] Peter B. Kang,[1,6] Frederic Shapiro,[7] Fedik Rahimov,[1,2] Genri Kawahara,[1,2] Jeffrey J. Widrick,[1] and Louis M. Kunkel[1,2,8,9]

[1]Division of Genetics and Genomics, Boston Children's Hospital, Boston, Massachusetts, USA. [2]Department of Pediatrics and Genetics, Harvard Medical School, Boston, Massachusetts, USA. [3]Departamento de Neurología, Escuela de Medicina, Pontificia Universidad Católica de Chile, Santiago, RM, Chile. [4]Stem Cell Institute, Paul and Sheila Wellstone Muscular Dystrophy Center, Department of Neurology, University of Minnesota Medical School, Minneapolis, Minnesota, USA. [5]Center for Human Placenta Research, Department of Obstetrics and Gynecology, Hadassah-Hebrew University Medical Center, Mt. Scopus Jerusalem, Israel. [6]Department of Neurology and [7]Department of Orthopedic Surgery, Boston Children's Hospital and Harvard Medical School, Boston, Massachusetts, USA. [8]The Manton Center for Orphan Disease Research, Boston Children's Hospital, Boston, Massachusetts, USA. [9]Harvard Stem Cell Institute, Cambridge, Massachusetts, USA.

Duchenne muscular dystrophy (DMD) is caused by mutations in the gene encoding dystrophin, which results in dysfunctional signaling pathways within muscle. Previously, we identified microRNA-486 (miR-486) as a muscle-enriched microRNA that is markedly reduced in the muscles of dystrophin-deficient mice (*Dmd*$^{mdx\text{-}5Cv}$ mice) and in DMD patient muscles. Here, we determined that muscle-specific transgenic overexpression of miR-486 in muscle of *Dmd*$^{mdx\text{-}5Cv}$ mice results in reduced serum creatine kinase levels, improved sarcolemmal integrity, fewer centralized myonuclei, increased myofiber size, and improved muscle physiology and performance. Additionally, we identified dedicator of cytokinesis 3 (DOCK3) as a miR-486 target in skeletal muscle and determined that DOCK3 expression is induced in dystrophic muscles. DOCK3 overexpression in human myotubes modulated PTEN/AKT signaling, which regulates muscle hypertrophy and growth, and induced apoptosis. Furthermore, several components of the PTEN/AKT pathway were markedly modulated by miR-486 in dystrophin-deficient muscle. Skeletal muscle–specific miR-486 overexpression in *Dmd*$^{mdx\text{-}5Cv}$ animals decreased levels of DOCK3, reduced PTEN expression, and subsequently increased levels of phosphorylated AKT, which resulted in an overall beneficial effect. Together, these studies demonstrate that stable overexpression of miR-486 ameliorates the disease progression of dystrophin-deficient skeletal muscle.

Introduction

Mammalian skeletal muscle is a dynamic organ capable of repairing itself following injury or atrophy arising from prolonged disuse. The skeletal muscle–regenerative process is a well-regulated process involving a variety of muscle progenitor cells and signaling molecules that work systematically to repair the damaged myofiber. The skeletal muscles of Duchenne muscular dystrophy (DMD) patients undergo waves or cycles of degeneration followed by regeneration, muscle tearing, and inflammation that lead to progressive muscle weakness and multi-organ complications, among which respiratory failure and cardiomyopathy are life threatening (1). There have been several novel approaches to treating the disease, such as the use of exon-skipping morpholinos or 2′-O-methyl phosphorothioate (2′OmePS) antisense oligonucleotides (AONs), which restore a truncated dystrophin open reading frame (ORFs) (2–5). While these therapeutic strategies have shown promise in human clinical trials, the long-term functional consequences of these treatments have yet to be fully elucidated (3, 6). Additional strategies are needed to treat the already damaged muscle and dysregulated secondary signaling pathways that exist due to chronic dystrophin deficiency (6–8). One strategy that has shown beneficial effects in dystrophin-deficient animal models is the modulation of components of the PTEN/AKT signaling pathway (9–11). PTEN, a tumor suppressor gene with diverse functions in multiple tissues, is induced in dystrophin-deficient muscle (12–14). This increase in *Pten* expression levels is accompanied by a subsequent reduction in phosphorylated *Akt*, both of which have been shown to regulate glucose and insulin signaling pathways in skeletal muscle (15–19). Transgenic overexpression of a constitutively active version of *Akt* in skeletal muscle resulted in muscle hypertrophy and improved muscle histology and physiology in *Dmd*^{mdx} mice (9, 10, 20). Direct suppression of *Pten* in mouse myoblasts increased myogenic differentiation with a subsequent increase in phosphorylated *Akt* (21). Ablation of *Pten* exclusively in mouse skeletal muscle resulted in leaner muscle and an improved ability to regenerate muscle on a high-fat diet (22).

To identify novel therapies and targets for treating dystrophin-deficient skeletal muscle, animal models have been proven to be useful (23). The *Dmd*^{mdx} mouse contains a spontaneous nonsense

Conflict of interest: Louis M. Kunkel is a consultant for Pfizer Inc., Summit Corporation PLC, and Tarix Pharmaceuticals for muscle disease drug therapies and for SynapDx Corporation for autism screening technologies. Peter B. Kang was previously a coinvestigator on a study funded by ISIS Pharmaceuticals, was a consultant for Third Rock Ventures, and serves on the DMD Advisory Board of Sarepta Therapeutics.

Citation for this article: *J Clin Invest.* 2014;124(6):2651–2667. doi:10.1172/JCI73579.

mutation in exon 23 of the mouse Dystrophin (*Dmd*) gene and has been shown to have muscle deficits associated with dystrophin deficiency (24–26). An ENU-mutagenesis screen later identified several additional mouse strains containing mutations elsewhere in the mouse *Dmd* gene (27). One strain of dystrophic mice from that screen, $Dmd^{mdx\text{-}5Cv}$, contains a nonsense mutation in exon 10, shows the fewest number of revertant fibers among all the Dmd^{mdx} mouse strains, and has a severe diaphragm muscle-force deficit (28, 29). Given the severity of the disease phenotypes observed in the $Dmd^{mdx\text{-}5Cv}$ mice, this mouse strain is highly useful for testing novel drug compounds and factors that might ameliorate clinical pathological aspects of dystrophin deficiency in an animal model.

MicroRNAs are 21–24 nucleotide small RNAs that have been shown to regulate gene expression by either degrading their target mRNA or interfering with the ribosome's ability to translate the target mRNA (30). MicroRNAs can regulate several target genes in a single pathway or multiple signaling pathways at critical time points in development and disease progression (31–34). The ability to quickly modulate the expression levels of disease-relevant microRNAs using viral overexpression or antisense inhibitors, makes microRNA-based therapies an attractive therapy for the treatment of complex diseases in which many signaling pathways are significantly affected. Previously, we identified the microRNA microRNA-486 (miR-486) as being significantly reduced in expression levels in dystrophin-deficient DMD muscle, but not in the milder Becker muscular dystrophy (BMD) muscle (35, 36). miR-486 is highly enriched in muscle, and may promote myogenic differentiation by downregulating the expression of the transcription factor Pax7 in skeletal muscle satellite cells (37, 38). Here, we show that transgenic overexpression of miR-486 in the muscles of dystrophic ($Dmd^{mdx\text{-}5Cv}$) mice ameliorates many of the clinical signs associated with dystrophin deficiency. Dystrophic mice that overexpress miR-486 have reduced serum creatine kinase (CK) levels, improved muscle physiology, and improved muscle performance. Additionally, we show that miR-486 overexpression directly modulates the PTEN/AKT signaling pathway in normal and dystrophic mouse muscle. Finally, we identify dedicator of cytokinesis 3 (DOCK3) (also called modifier of cell adhesion [MOCA]) as a direct target of miR-486 in normal and dystrophic muscles and show that it plays a functional role in myotube survival. Together, these studies identify miR-486 as a modulator of disease pathology in dystrophic skeletal muscle and open up the possibility of using miR-486 overexpression as a potential novel therapy for muscular dystrophy.

Results

miR-486 is enriched in myogenic tissues but reduced in dystrophic muscle. Previously, we identified miR-486 as being strongly reduced in expression levels in human dystrophic muscle (35, 36). miR-486 expression is highly enriched in developing mouse muscle and is induced during myogenic differentiation of muscle stem cells (36–38). We first sought to examine the expression of human miR-486 (hsa-miR-486), specifically the human miR-486-5p sequence, in a panel of normal adult tissues (Sanger miRBase: http://mirbase.org/). Human miR-486-5p was expressed at the highest levels in the skeletal muscle and heart tissues and at more moderate levels in lung, brain, and bladder (Supplemental Figure 1A; supplemental material available online with this article; doi:10.1172/JCI73579DS1). To confirm these findings in another mammalian organism, we analyzed a similar array of adult mouse tissues for miR-486-5p expression levels. Mouse miR-486-5p was similarly enriched in the adult heart and skeletal muscles while also showing moderate expression in the brain and bladder tissues (Supplemental Figure 1B). Given the similarities between mouse and human miR-486 expression, we next analyzed the pattern of miR-486 in both oxidative and glycolytic muscle groups consisting of the tibialis anterior (TA), extensor digitorum longus (EDL), gastrocnemius, soleus, triceps, paraspinal muscles, and the diaphragm in both normal and dystrophin-deficient ($Dmd^{mdx\text{-}5Cv}$ strain) muscles. miR-486 was expressed in all 7 of the muscle groups analyzed, but reduced in expression in all of the $Dmd^{mdx\text{-}5Cv}$ muscles except for the paraspinal muscles (Supplemental Figure 1C). These results in murine dystrophin-deficient muscle are in agreement with our previous finding that miR-486 transcript levels are strongly reduced in human DMD muscle biopsies (35, 36).

Muscle-specific overexpression of miR-486 improves skeletal muscle histology in dystrophic muscle. Suppression of miR-21, a fibroblast-proliferation–inducing microRNA that is induced in dystrophin-deficient muscle, resulted in improved pathology in Dmd^{mdx} mouse muscles through modulation of the PTEN/AKT signaling pathway (39). Thus, we postulated that overexpression of a microRNA that is reduced in dystrophic muscle, miR-486, might have a similar beneficial effect in delaying or ameliorating some of the signs of muscular dystrophy in $Dmd^{mdx\text{-}5Cv}$ mice. To determine the functional consequences of miR-486 overexpression in muscle on a dystrophic background, we mated the Tg(*Cmk-Mir486*) (MCK promoter) mice with the $Dmd^{mdx\text{-}5Cv}$ mice. We performed histological analysis of the muscles of the $Dmd^{mdx\text{-}5Cv}$ Tg(*Cmk-Mir486*) adult (2 to 4 months old) mice to determine what effect or effects miR-486 overexpression might have on disease progression. Centralized myonuclei are indicative of dystrophin deficiency in mice and can be used as an indicator of myofiber regeneration (23, 25). The TA and diaphragm muscles of $Dmd^{mdx\text{-}5Cv}$ Tg(*Cmk-Mir486*) mice revealed reduced numbers of centralized myonuclei compared with their $Dmd^{mdx\text{-}5Cv}$ control littermates (Figure 1, A and B). Histological examination of the gastrocnemius muscles from adult $Dmd^{mdx\text{-}5Cv}$ Tg(*Cmk-Mir486*) mice also displayed improved overall histology and reduced numbers of centralized myonuclei, further supporting a functional role for miR-486 overexpression as a means of delaying the disease progression of muscular dystrophy (Supplemental Figure 2, A and B). A previous study has shown that the diaphragm muscle of the $Dmd^{mdx\text{-}5Cv}$ strain is more severely affected by dystrophin deficiency than other muscles (29). We measured the muscle fiber cross-sectional area (CSA) in WT, Tg(*Cmk-Mir486*), $Dmd^{mdx\text{-}5Cv}$, and $Dmd^{mdx\text{-}5Cv}$ Tg(*Cmk-Mir486*) mice to determine what effects miR-486 might have on overall myofiber size. The Tg(*Cmk-Mir486*) mice displayed larger overall myofiber sizes when compared with their WT littermates, suggesting that miR-486 might be inducing myofiber hypertrophy (Figure 1C). Similarly, the $Dmd^{mdx\text{-}5Cv}$ Tg(*Cmk-Mir486*) showed significantly larger myofibers compared with their $Dmd^{mdx\text{-}5Cv}$ littermates, comparable in size to WT myofibers (Figure 1C). Thus, the overall histology of $Dmd^{mdx\text{-}5Cv}$ dystrophic mice that overexpress the miR-486 transgene was greatly improved when compared with their $Dmd^{mdx\text{-}5Cv}$ littermates.

miR-486 overexpressing mice have improved serum biochemistries and reduced muscle membrane permeability. We next tested myofiber membrane permeability using an Evans blue dye (EBD) uptake assay that is often used to quantify the degree of myofiber damage in Dmd^{mdx} mice (40, 41). The $Dmd^{mdx\text{-}5Cv}$ Tg(*Cmk-Mir486*) mice showed signifi-

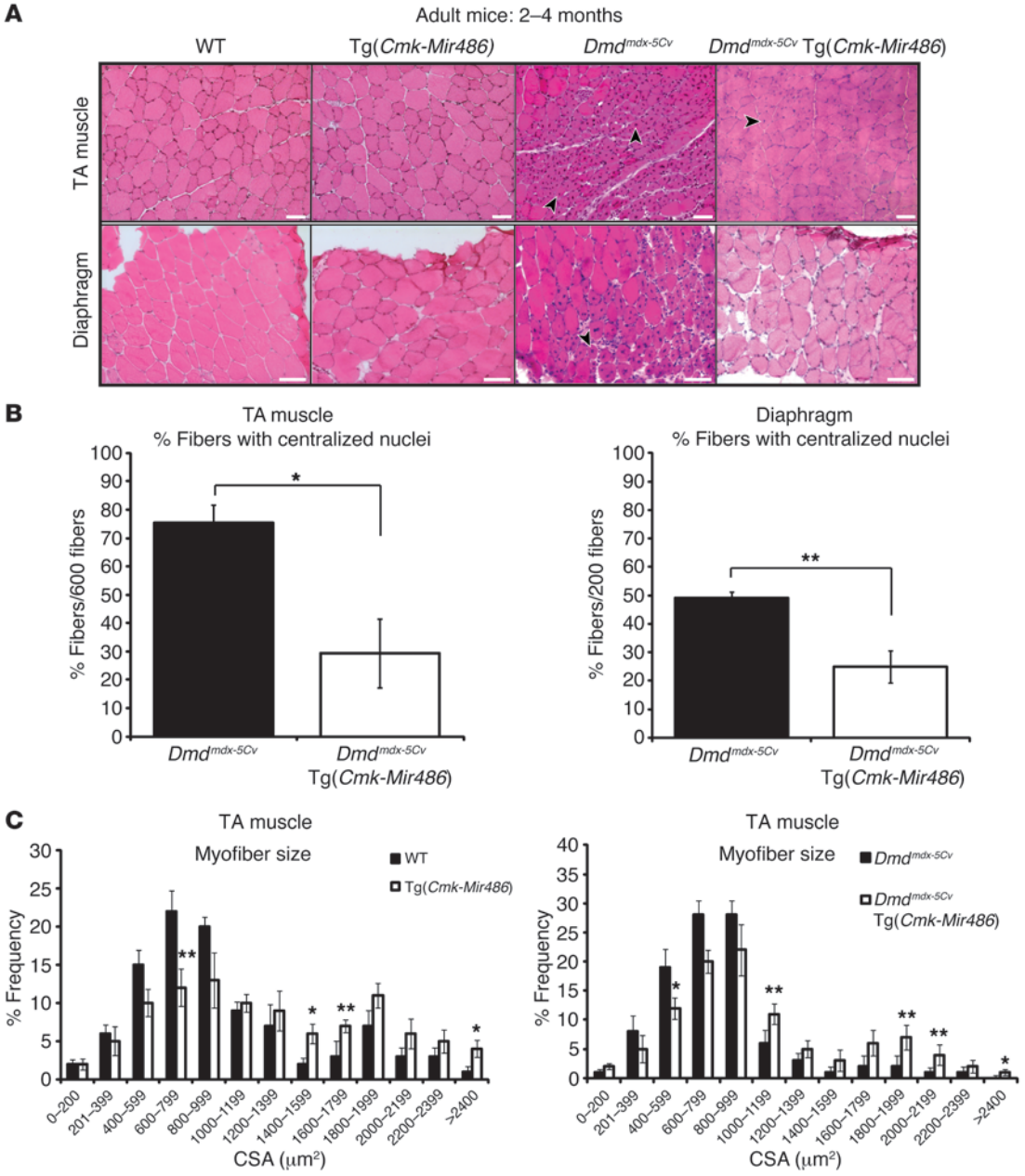

Figure 1

Overexpression of miR-486 in dystrophic *Dmd*$^{mdx\text{-}5Cv}$ mouse muscles reduces dystrophic disease histopathology. (**A**) H&E staining of adult TA and diaphragm muscles from WT, Tg(*Cmk-Mir486*), *Dmd*$^{mdx\text{-}5Cv}$, and *Dmd*$^{mdx\text{-}5Cv}$ Tg(*Cmk-Mir486*) mice. Arrowheads demarcate centralized nuclei, a classic finding in dystrophic disease and regenerating skeletal muscle. Scale bars: 50 μm. (**B**) Summary graphs of centralized nuclei counted from the TA and diaphragm muscles of adult *Dmd*$^{mdx\text{-}5Cv}$ and *Dmd*$^{mdx\text{-}5Cv}$ Tg(*Cmk-Mir486*) mice. (**C**) Fiber type cross-section area analysis of the TA muscles of WT, Tg(*Cmk-Mir486*), *Dmd*$^{mdx\text{-}5Cv}$, and *Dmd*$^{mdx\text{-}5Cv}$ Tg(*Cmk-Mir486*) adult mice. Six-hundred fibers from 5 separate mice per cohort were used for analysis. **P* < 0.005; ***P* < 0.05. The mean and SEM values for the 4 genotype cohorts are as follows: WT (773 ± 27), Tg(*Cmk-Mir486*) (907 ± 19), *Dmd*$^{mdx\text{-}5Cv}$(691 ± 42), and *Dmd*$^{mdx\text{-}5Cv}$ Tg(*Cmk-Mir486*) (815 ± 36) measured in μm².

cantly less EBD infiltration in their TA muscles than their *Dmd*$^{mdx\text{-}5Cv}$ littermates, suggesting that miR-486 overexpression ameliorated myofiber damage (Figure 2, A and B). These results were also observed in the gastrocnemius muscles, indicating that miR-486 muscle overexpression may have beneficial effects in preventing muscle membrane permeability and overall membrane instability that is often associated with loss of dystrophin (Figure 2C). Dysregulated serum biomarkers, such as CK and alanine transaminase (ALT), are hallmarks of dystrophic muscle and are often used to diagnose the severity of muscle disease in both humans and mice (23, 42–44). We next measured the levels of serum CK in adult WT, Tg(*Cmk-Mir486*), *Dmd*$^{mdx\text{-}5Cv}$, and *Dmd*$^{mdx\text{-}5Cv}$ Tg(*Cmk-Mir486*) mice. There were no significant differences in levels of serum CK between WT and Tg(*Cmk-Mir486*) mice; however, *Dmd*$^{mdx\text{-}5Cv}$ mice showed

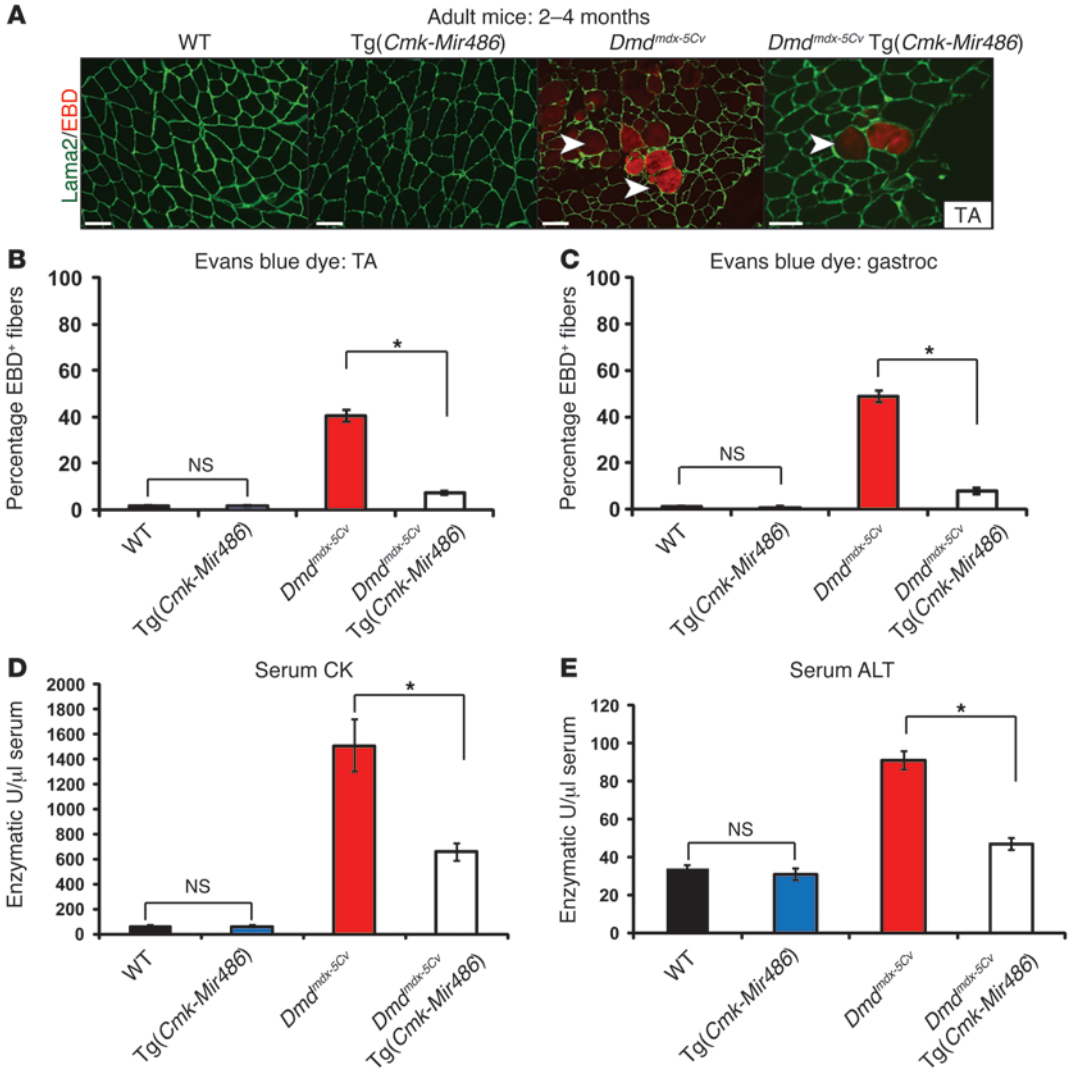

Figure 2

Dmd$^{mdx\text{-}5Cv}$ Tg(*Cmk-Mir486*) mice have improved muscle membrane integrity and serum biochemistry. (**A**) EBD (red fluorescence) immunohistochemistry of TA muscle biopsies taken from WT, Tg(*Cmk-Mir486*), *Dmd*$^{mdx\text{-}5Cv}$, and *Dmd*$^{mdx\text{-}5Cv}$ Tg(*Cmk-Mir486*) mice. Sections were costained with Laminin α-2 antisera (Lama2; green) to demarcate the myofiber basal lamina. Arrowheads demarcate EBD-positive myofibers. Scale bars: 50 μm. (**B** and **C**) Graph showing the quantification of EBD-positive myofibers from the TA (**B**) and gastrocnemius (**C**) muscles in WT (black bars), Tg(*Cmk-Mir486*) (blue bars), *Dmd*$^{mdx\text{-}5Cv}$ (red bars), and *Dmd*$^{mdx\text{-}5Cv}$ Tg(*Cmk-Mir486*) (white bars) mice. Six-hundred fibers from 3 separate mice per cohort were quantified. (**D** and **E**) Serum CK and ALT enzymatic levels (measured as enzymatic units per μl) taken from the 4 genotype cohorts (n = 5 mice per genotype cohort used). *P < 0.05. Gastroc, gastrocnemius.

approximately 20-fold higher levels of serum CK as compared with WT mice (Figure 2D). Remarkably, the levels of serum CK were reduced by half in adult *Dmd*$^{mdx\text{-}5Cv}$ Tg(*Cmk-Mir486*) mice, again suggesting decreased membrane permeability (Figure 2D). Similarly, the levels of ALT were also reduced in *Dmd*$^{mdx\text{-}5Cv}$ Tg(*Cmk-Mir486*) mice when compared with *Dmd*$^{mdx\text{-}5Cv}$ littermates (Figure 2E). Together, these results demonstrate that miR-486 muscle overexpression improves the serum biomarkers that are typically dysregulated in dystrophic mouse muscle toward near normal levels.

Overexpression of miR-486 improves Dmd$^{mdx\text{-}5Cv}$ *muscle physiological function*. To determine whether miR-486 overexpression would improve muscle physiological function, we tested age-matched WT, Tg(*Cmk-Mir486*), *Dmd*$^{mdx\text{-}5Cv}$, and *Dmd*$^{mdx\text{-}5Cv}$ Tg(*Cmk-Mir486*) mice using a series of treadmill, grip strength, activity, and isolated muscle-force output assays. As expected, *Dmd*$^{mdx\text{-}5Cv}$ mice performed poorly on the treadmill assay compared with WT and Tg(*Cmk-Mir486*) mice in both the time to overall exhaustion and total distance tests (Figure 3, A and B). The *Dmd*$^{mdx\text{-}5Cv}$ Tg(*Cmk-Mir486*) mice showed marked improvements in both total running distances and time to exhaustion compared with *Dmd*$^{mdx\text{-}5Cv}$ littermates (Figure 3, A and B). Previous studies have shown that *Dmd*^{mdx} mice have reduced overall and vertical activity before and after forced exercise (45, 46). We measured the total activity of all 4 mouse genotype cohorts before and after forced downhill treadmill exercise. While *Dmd*$^{mdx\text{-}5Cv}$ mice showed severe decreases in overall and vertical activity before and after forced exercise, the *Dmd*$^{mdx\text{-}5Cv}$ Tg(*Cmk-Mir486*) mice displayed activity patterns similar to those of both WT and Tg(*Cmk-Mir486*) mice (Figure 3, C and D).

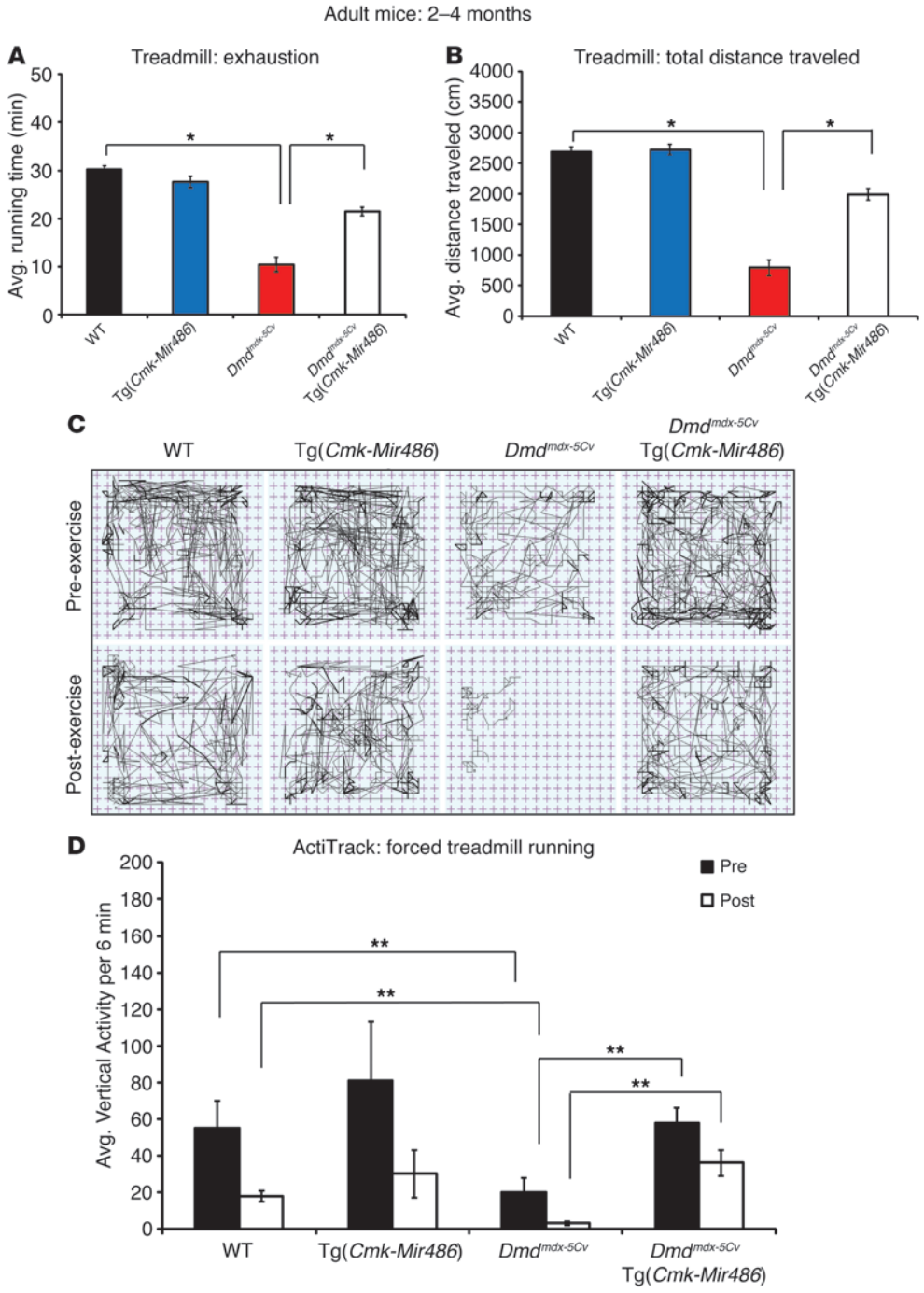

Figure 3
miR-486 overexpression in $Dmd^{mdx\text{-}5Cv}$ mice improves dystrophic muscle physiology. (**A**) Graph of forced downhill treadmill running of WT (black bars), Tg(*Cmk-Mir486*) (blue bars), $Dmd^{mdx\text{-}5Cv}$ (red bars), and $Dmd^{mdx\text{-}5Cv}$ Tg(*Cmk-Mir486*) (white bars) mice measuring time of endurance (total time before the mice reached exhaustion) in minutes. (**B**) Graph of forced downhill treadmill running measuring total distance traveled in centimeters (cm) of the 4 genotype cohorts. (**C**) Representative ActiTrack activity plots of the 4 mouse genotype cohorts measured before (pre-exercise) and after (post-exercise) forced downhill treadmill running. Thin lines represent mouse distance traveled, while darker lines represent instances of rearing (vertical activity). (**D**) Summary graph plotting the total number of instances of rearing (vertical activity) of mice before and after forced treadmill running. $^{*}P < 0.005$; $^{**}P < 0.05$.

miR-486 overexpression improves $Dmd^{mdx\text{-}5Cv}$ muscle strength and tetanic force output. We tested cage-grip strength (the total force of a mouse's front paws to grasp a wire cage) in the 4 mouse genotype cohorts as an in vivo output of muscle strength. The Tg(*Cmk-Mir486*) mice generated similar overall cage-grip force output when compared with WT controls (Figure 4A). More importantly, $Dmd^{mdx\text{-}5Cv}$ Tg (*Cmk-Mir486*) mice showed a significant increase in the overall force output and were able to hold onto their cages for longer periods of time compared with $Dmd^{mdx\text{-}5Cv}$ littermates (Figure 4, A and B). These findings demonstrate that loss of muscle-force output in dystrophin deficiency is significantly improved when miR-486 is overexpressed. We next performed physiological assays on isolated groups of muscles (EDL, soleus, and diaphragm strips) biopsied from adult WT, Tg(*Cmk-Mir486*), $Dmd^{mdx\text{-}5Cv}$, and $Dmd^{mdx\text{-}5Cv}$ Tg(*Cmk-Mir486*) age-matched cohorts. The specific force (tetanic force per muscle physiological CSA) of EDL, soleus, and diaphragm muscles is reduced in Dmd^{mdx} and $Dmd^{mdx\text{-}5Cv}$ mice (29, 47). We observed no significant differences in specific force in the muscles of WT versus Tg(*Cmk-Mir486*) mice, but a marked improvement in the muscles from $Dmd^{mdx\text{-}5Cv}$ Tg(*Cmk-Mir486*) mice when directly compared with $Dmd^{mdx\text{-}5Cv}$ littermates (Figure 4C). These studies demonstrate

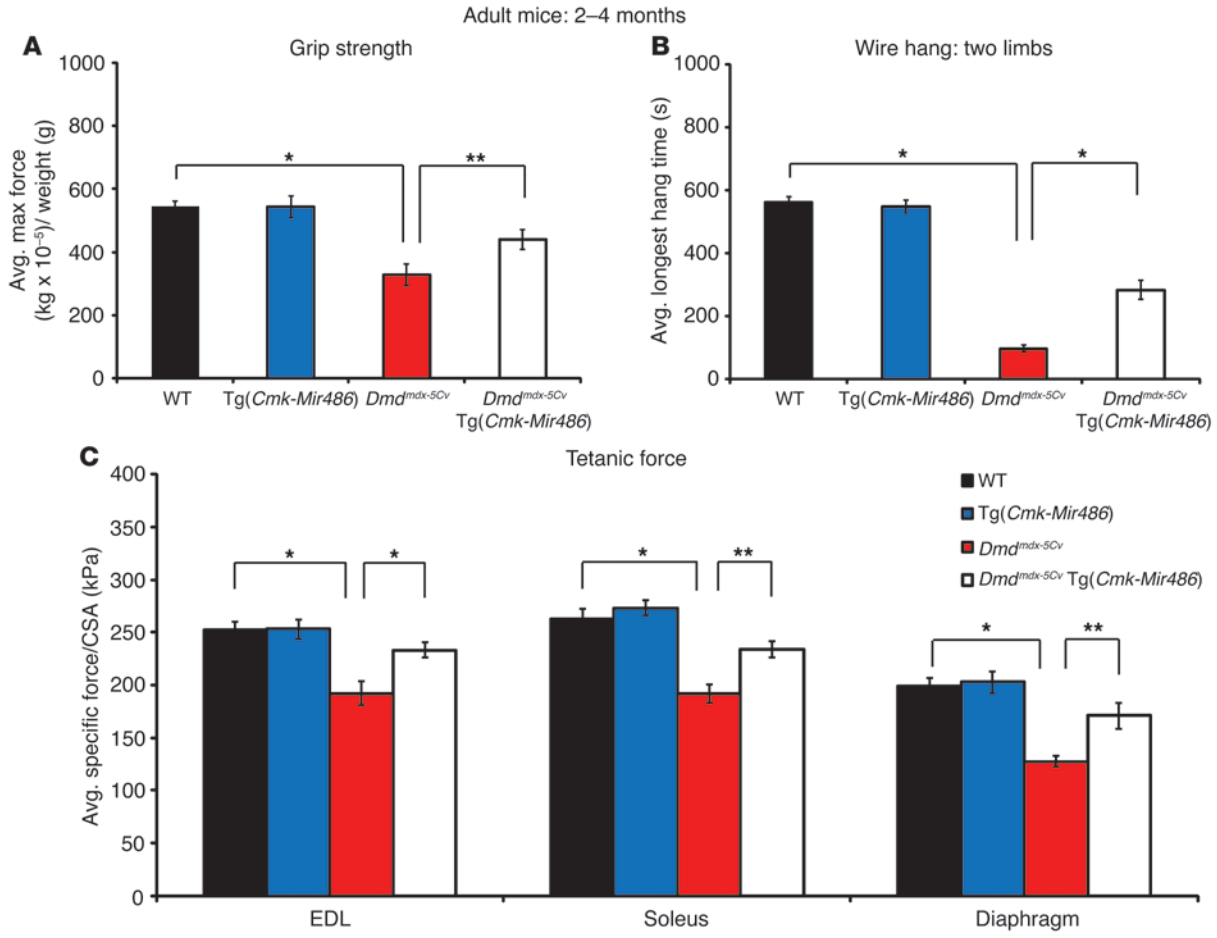

Figure 4

miR-486–overexpressing dystrophic muscles have improved strength and tetanic force outputs. (**A**) Cage-grip strength measurements of mice of the 4 genotype cohorts measured as kg × 10^{-5} and normalized to mouse weight (grams). (**B**) Two-limb (forelimbs) wire hang-time measurements (seconds) of each of the 4 genotype cohorts. (**C**) Tetanic muscle-force measurements, normalized to CSA, of isolated EDL, soleus, and diaphragm muscles. Eight (WT and Tg[*Cmk-Mir486*]) and 12 (*Dmd*$^{mdx\text{-}5Cv}$ and *Dmd*$^{mdx\text{-}5Cv}$ Tg[*Cmk-Mir486*]) adult (2 to 4 months old) male mice were used for each genotype cohort. *$P < 0.005$; **$P < 0.05$.

that muscle-force output is improved in the murine muscles that overexpress miR-486 on the *Dmd*$^{mdx\text{-}5Cv}$ background.

Skeletal muscle fiber types are not significantly affected by miR-486 overexpression. In DMD muscle, the fast twitch type II fibers are the first group to break down, while the slow type I fibers remain are the last group to be affected (48). A previous study of skeletal muscle fiber types revealed a greater number of slow, type I fibers in the soleus muscles of *Dmd*$^{mdx\text{-}5Cv}$ mice (49). We tested whether any of the beneficial effects observed in the *Dmd*$^{mdx\text{-}5Cv}$ Tg(*Cmk-Mir486*) mice might be due to changes in muscle fiber type composition. Using immunofluorescence staining with monoclonal myosin heavy chain antibodies, we counted the total numbers of type I, type IIa, and type IIb in adult (2 to 4 months old) WT, Tg(*Cmk-Mir486*), *Dmd*$^{mdx\text{-}5Cv}$, and *Dmd*$^{mdx\text{-}5Cv}$ Tg(*Cmk-Mir486*) age-matched cohorts (50). As expected, we observed a shift from fast to slow type myofibers in the soleus muscles of *Dmd*$^{mdx\text{-}5Cv}$ mice when compared with their age-matched WT cohort (Supplemental Figure 3, A and B). We did observe a slight overall increase in the number of type IIa oxidative fibers and a corresponding decrease in the number of type IIb glycolytic fibers in the TA muscles of the Tg(*Cmk-Mir486*) mice (Supplemental Figure 3A). Previous studies have shown that alterations of the PTEN/AKT signaling components in mouse muscles, while inducing muscle hypertrophy, had very modest effects on muscle fiber type specification (51–53). Thus, it is likely that the alteration of fiber type composition in miR-486–overexpressing mice might be due to the changes in expression levels of signaling components including the PTEN/AKT pathway. However, no change in the fiber type distribution was observed when *Dmd*$^{mdx\text{-}5Cv}$ and *Dmd*$^{mdx\text{-}5Cv}$ Tg(*Cmk-Mir486*) soleus, TA, or gastrocnemius muscles were compared (Supplemental Figure 3, A and B). These findings suggest that the beneficial effects seen in miR-486–overexpressing *Dmd*$^{mdx\text{-}5Cv}$ mice are most likely independent of any significant changes in muscle fiber type composition.

Aged dystrophic mice show similar beneficial effects in their muscles resulting from miR-486 transgenic overexpression. It has been well documented that dystrophic disease symptoms, such as muscle weakness, increased serum CK levels, and loss of muscle force, occur in aged *Dmd*^{mdx} mice (54). In the more severe dystrophic *Dmd*$^{mdx\text{-}5Cv}$ mice, muscle fatigue and functional deficits have been reported as early as 8 weeks and progressively worsen in mice that have been

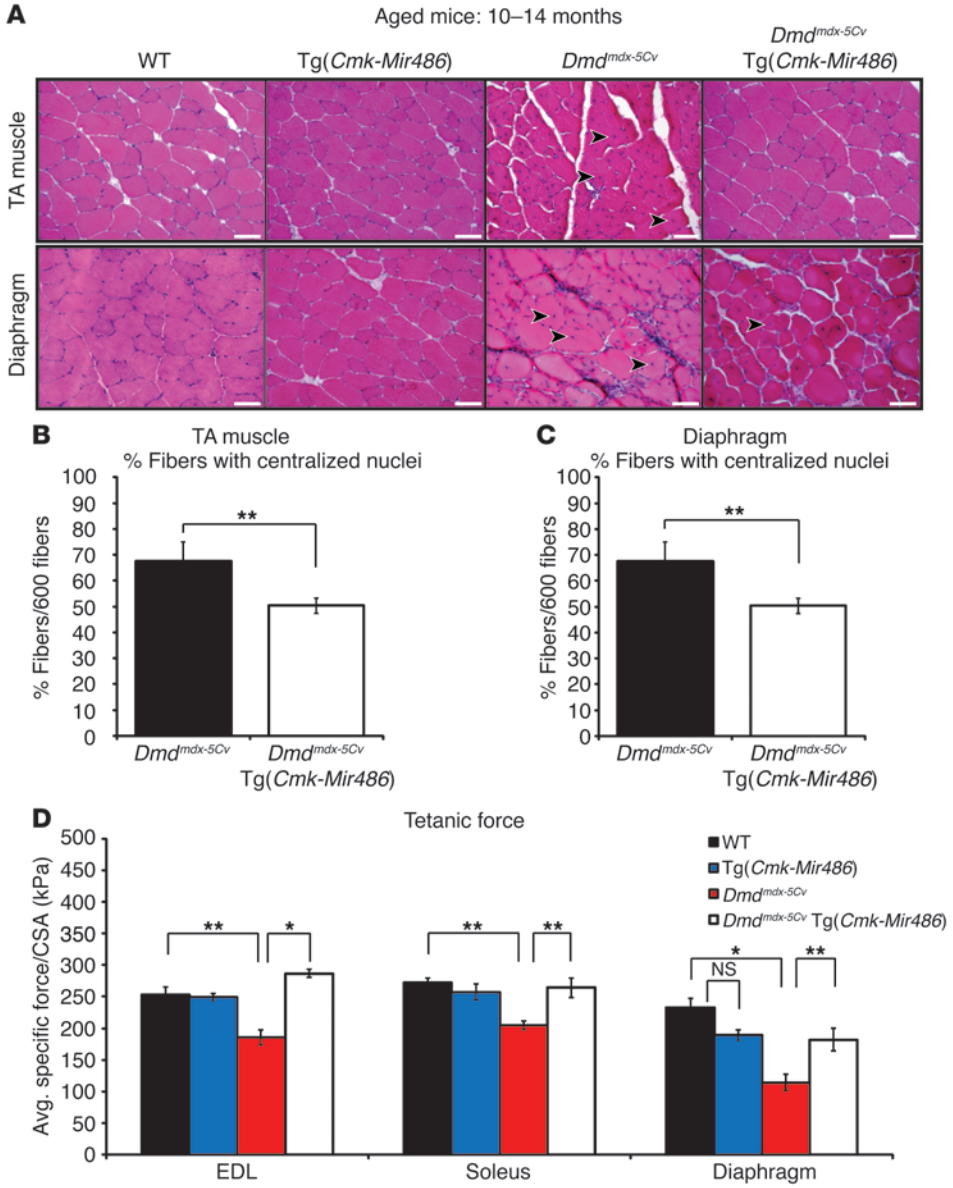

Figure 5
Aged dystrophic mice show similar improved pathology resulting from miR-486 transgenic overexpression. (**A**) Representative H&E staining of TA and diaphragm muscles taken from aged (10 to 14 months old) WT, Tg(*Cmk-Mir486*), *Dmd*$^{mdx\text{-}5Cv}$, and *Dmd*$^{mdx\text{-}5Cv}$ Tg(*Cmk-Mir486*) mice. Arrowheads represent centralized myonuclei. Scale bars: 50 μm. (**B**) Graphs of centralized myonuclei counts of the TA and (**C**) diaphragm muscles of aged *Dmd*$^{mdx\text{-}5Cv}$ and *Dmd*$^{mdx\text{-}5Cv}$ Tg(*Cmk-Mir486*) mice. Three mice (n = 6 TA and n = 3 diaphragm muscles) were used, with 600 TA and 200 diaphragm individual myofibers being counted. (**D**) Tetanic muscle-force measurements, normalized to CSA, of isolated EDL, soleus, and diaphragm muscles. Five (WT and Tg[*Cmk-Mir486*]) to 8 (*Dmd*$^{mdx\text{-}5Cv}$ and *Dmd*$^{mdx\text{-}5Cv}$ Tg[*Cmk-Mir486*]) aged (10 to 14 months old) male mice were used for each genotype cohort. $^{*}P < 0.005$; $^{**}P < 0.05$.

aged to 1 year (29). To determine whether the beneficial effects observed in the adult 2- to 4-month-old mice were maintained in aged dystrophic muscles, we performed similar histological, biochemical, and physiological measurements on aged *Dmd*$^{mdx\text{-}5Cv}$ (10 to 14 months old) mice that overexpressed the miR-486 transgene. We observed a similar decrease in the amount of central myonuclei and overall improved histology of the TA muscles and diaphragm in aged *Dmd*$^{mdx\text{-}5Cv}$ Tg(*Cmk-Mir486*) mice when compared with their *Dmd*$^{mdx\text{-}5Cv}$ littermates (Figure 5, A–C). Additionally, serum profiling of aged *Dmd*$^{mdx\text{-}5Cv}$ Tg(*Cmk-Mir486*) mice revealed a similar reduction in the overall serum CK levels when compared with the dystrophic *Dmd*$^{mdx\text{-}5Cv}$ littermates (Supplemental Figure 4, A and B). Finally, we measured the specific force of the EDL, soleus, and diaphragm muscles from aged *Dmd*$^{mdx\text{-}5Cv}$ Tg(*Cmk-Mir486*) and *Dmd*$^{mdx\text{-}5Cv}$ mice along with aged WT and Tg(*Cmk-Mir486*) controls. We observed that the aged *Dmd*$^{mdx\text{-}5Cv}$ Tg(*Cmk-Mir486*) mice had maintained their specific muscle strength, similar to that of WT and Tg(*Cmk-Mir486*) mice, when compared with their *Dmd*$^{mdx\text{-}5Cv}$ littermates (Figure 5D). Together, these studies demonstrate that the beneficial effects observed with the overexpression of miR-486 in the skeletal muscles of *Dmd*$^{mdx\text{-}5Cv}$ mice are maintained in older dystrophic mice.

Overexpression of miR-486 reduces Pten expression while increasing phosphorylated Akt levels in skeletal muscle. miR-486 was previously shown to target PTEN and PTEN/AKT signaling components in both heart and skeletal muscles (36, 37, 55). We next measured the protein levels of PTEN and AKT directly in the TA muscles of both WT and *Dmd*$^{mdx\text{-}5Cv}$ mice, which overexpress miR-486. Overexpression of miR-486 strongly reduced the expression of *Pten* in the muscles of Tg(*Cmk-Mir486*) mice compared with their WT control littermates (Figure 6, A and B). Similarly, the overall protein levels of *Pten* in the *Dmd*$^{mdx\text{-}5Cv}$ Tg(*Cmk-Mir486*) mice were also reduced compared with the levels in their *Dmd*$^{mdx\text{-}5Cv}$ littermates, implicating *Pten* as a direct in vivo target of miR-486 in skeletal muscle (Figure 6, C and D). The total levels of all 3 Akt isoforms (Akt1/2/3) remained unchanged, while the levels

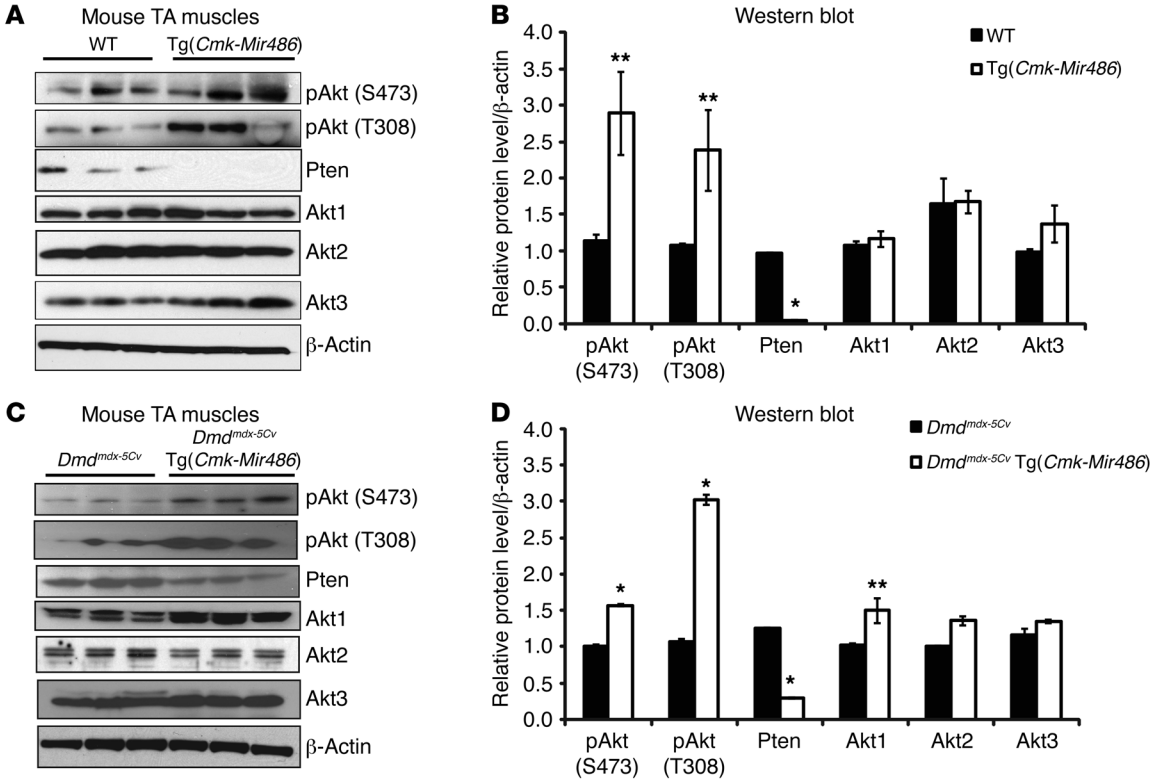

Figure 6

PTEN/AKT signaling is dysregulated in miR-486–overexpressing mouse muscle. (**A**) Western blot images of whole-tissue lysates from adult WT and Tg(*Cmk-Mir486*) mouse TA muscles. Three mice were used per genotype cohort. (**B**) Western blot densitometry values of phospho-AKT (S473), phospho-AKT (T308), AKT1/2/3, and PTEN protein images normalized to both the first lane and the β-actin–loading control. (**C**) Western blot images of whole-tissue lysates from adult *Dmd*$^{mdx\text{-}5Cv}$ and *Dmd*$^{mdx\text{-}5Cv}$ Tg(*Cmk-Mir486)*. Three mice were used per genotype cohort. (**D**) Western blot densitometry values of phospho-AKT (S473), phospho-AKT (T308), AKT1/2/3, and PTEN protein images normalized to both the first lane and the β-actin–loading control. *$P < 0.005$; **$P < 0.05$.

of phosphorylated AKT (S473 and T308) at 2 residues critical for its kinase function, significantly increased in the miR-486–overexpressing muscles (Figure 6, A–D). Thus, the overexpression of miR-486 in the skeletal muscles of Tg(*Cmk-Mir486*) mice significantly alters the expression levels of key components of the PTEN/AKT signaling pathway.

DOCK3 is a direct downstream target of miR-486 in skeletal muscle. To identify novel direct targets of miR-486 that might be modulating the pathology of dystrophic muscle, we utilized a bioinformatic approach using publically available software algorithms, which predict targets of microRNAs (TargetScan [www.targetscan.org], MicroCosm [http://www.ebi.ac.uk/enright-srv/microcosm/htdocs/targets/v5/], miRDB [http://mirdb.org/miRDB/]). We focused on predicted miR-486 targets whose mRNA transcripts were conversely elevated in DMD muscle and cross-referenced those targets with previously published DMD biopsy microarray data sets for mRNA transcripts that were elevated in DMD muscles (12, 56). Several miR-486–validated targets, including PTEN and FOXO1, were confirmed as elevated in DMD muscle by Western blot analysis (data not shown). One predicted target, DOCK3 (previously referred to as MOCA, modifier of cell adhesion), was found to be elevated in expression in DMD muscle biopsies (Figure 7A). The DOCK3 3′ UTR has a strongly evolutionarily conserved miR-486–binding seed site among mammals including mouse, dogs, and humans (Figure 7B). MicroRNAs can be functionally screened to determine whether they have repressive activity in cells by fusing the 3′ UTR of the miRNA target to luciferase, overexpressing the microRNA (or scrambled miR control), and measuring the amount of luciferase reporter activity. We cloned the human DOCK3 3′ UTR containing the miR-486 seed site to a luciferase reporter and transfected the construct into the nonmyogenic HEK293T cell line along with either miR-486 or scrambled miR control constructs and assayed for luciferase activity (Figure 7C). miR-486 suppressed human DOCK3 3′ UTR luciferase reporter activity when compared directly to scrambled miR controls (Figure 7D). Likewise, mutation of critical nucleotides in the miR-486 seed site of the DOCK3 3′ UTR resulted in the failure of miR-486 overexpression to suppress the luciferase levels of the reporter construct (Figure 7D). To test whether DOCK3 was a direct target of miR-486, we overexpressed miR-486 using either miR-486–overexpressing or scrambled miR control lentiviruses in normal human primary myotubes and analyzed DOCK3 protein levels. Overexpression of miR-486 inhibited endogenous DOCK3 protein levels in normal human primary myotubes (Figure 7E). Given the identification of *Dock3* mRNA transcript as a downstream target of miR-486 in skeletal muscle, we sought to measure DOCK3 expression levels during critical time points in myogenic differentiation. Human primary myoblasts from unaffected individuals and from

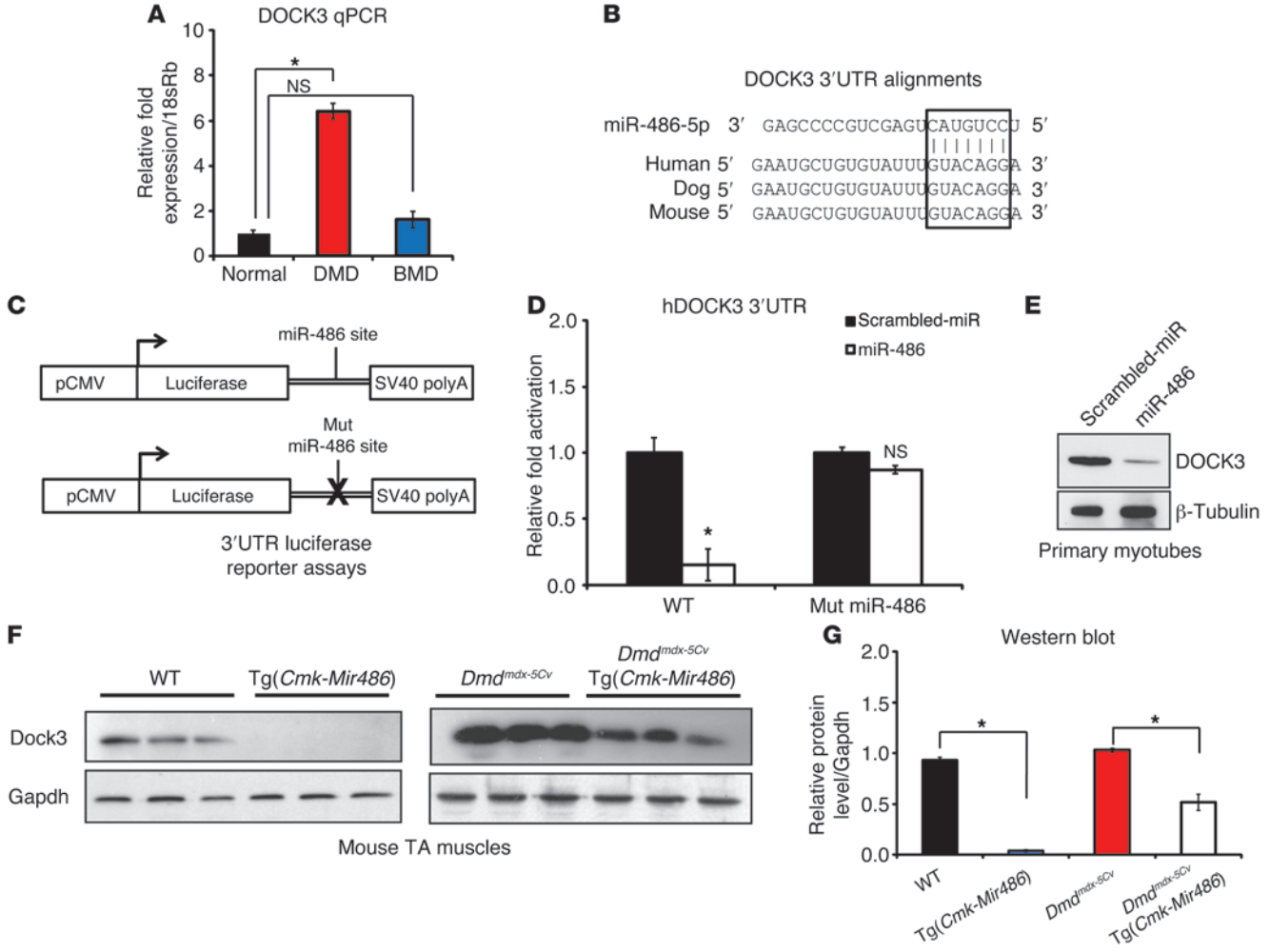

Figure 7

DOCK3 is a direct target of miR-486 in skeletal muscle. (**A**) Real-time qPCR of human DOCK3 expression levels in normal, DMD, and BMD muscle biopsies. Expression levels are normalized to the 18sRb loading control. (**B**) Evolutionary conservation of the miR-486 seed site in mammalian DOCK3 3′ UTRs. Human, dog, and mouse are shown aligned with the seed region of miR-486-5p (boxed inset). (**C**) Schematic of 3′ UTR of the miR-486 target fused to a luciferase reporter construct. The miR-486 seed site is mutated in the mutant constructs. (**D**) Relative luciferase fold expression of the human DOCK3 3′ UTR fused to luciferase and transfected into HEK293T cells with either miR-486 or scrambled miR control plasmids. (**E**) Western blot analysis of human DOCK3 protein expression in primary human myotubes overexpressing either miR-486 or scrambled miR control lentivirus. β-Tubulin is shown as a loading control. (**F**) Western blot of DOCK3 protein in WT, Tg(*Cmk-Mir486*), *Dmd*$^{mdx\text{-}5Cv}$, and *Dmd*$^{mdx\text{-}5Cv}$ Tg(*Cmk-Mir486*) TA muscle lysates. GAPDH is shown as a loading control. (**G**) Densitometry graph of DOCK3 protein expression normalized to either WT or *Dmd*$^{mdx\text{-}5Cv}$ levels,and the GAPDH loading control. *$P < 0.005$.

DMD patients were cultured in proliferative (high serum) conditions and induced to differentiate (low serum). DOCK3 transcript was not detectable under proliferative conditions, but was strongly increased in both normal and DMD muscle cells during later differentiation time points (Supplemental Figure 5A). Western blot analyses further confirmed the mRNA data (Supplemental Figure 5B). In comparison, DMD patient myoblasts showed significantly higher levels of DOCK3 protein expression at early myogenic differentiation time points and higher DOCK3 expression overall when compared with normal controls (Supplemental Figure 5B). Additionally, *Dock3* mRNA transcript levels were strongly increased in both normal and *Dmd*$^{mdx\text{-}5Cv}$ muscles during days 1 through 7 after cardiotoxin-induced TA muscle injuries (Supplemental Figure 5C). As found in human muscle biopsies, mouse *Dock3* transcript levels were significantly higher in the *Dmd*$^{mdx\text{-}5Cv}$ injured muscles as compared with WT controls. The time points of days 3 to 7 are characterized by highly regulated stages of muscle regeneration and myoblast fusion (57). Thus, it is possible that the increase in *Dock3* expression we observed suggests that *Dock3* might be an essential regulator of these processes during normal muscle regeneration. We next determined whether DOCK3 protein levels were reduced by miR-486 overexpression in vivo by measuring DOCK3 protein expression in the TA muscles of the Tg(*Cmk-Mir486*) mice. DOCK3 protein levels were reduced in Tg(*Cmk-Mir486*) mice in both the WT and *Dmd*$^{mdx\text{-}5Cv}$ background, supporting the conclusion that DOCK3 is regulated by miR-486 (Figure 7, F and G). These results demonstrate that DOCK3 is expressed at later time points of myogenic differentiation and

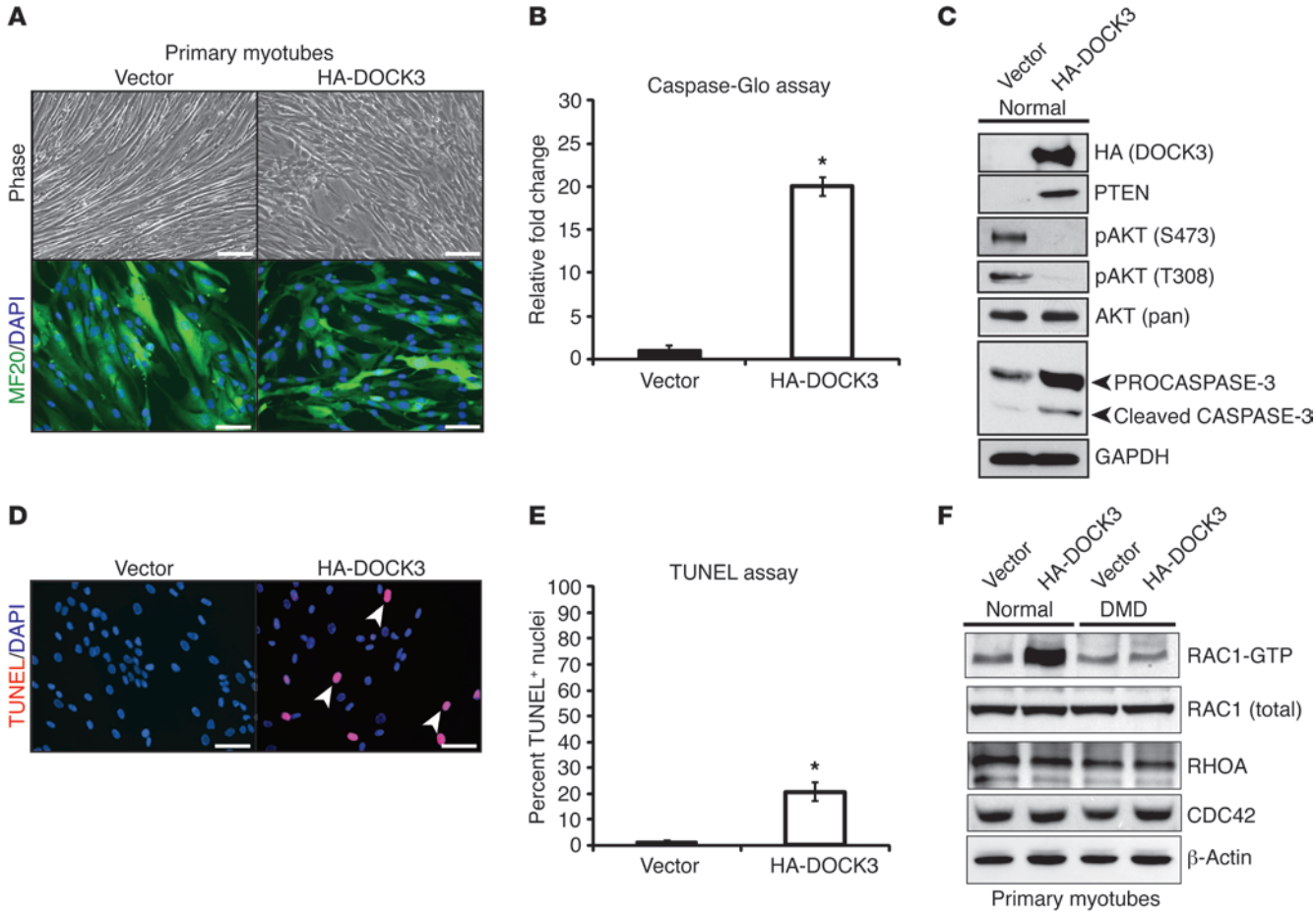

Figure 8

DOCK3 overexpression induces apoptosis and affects PTEN/AKT and RAC1/RHOA signaling in primary human myotubes. (**A**) Phase microscopy images of primary human myotubes expressing either a control vector (pCI-Neo) or HA-DOCK3. Stable-transfected (vector or HA-DOCK3) primary myoblasts were differentiated into myotubes by adding differentiation medium for 72 hours prior to imaging. Note the large phase-bright cell aggregates in the DOCK3-overexpressing primary myotubes as compared with vector controls. Scale bars: 100 μm. (**B**) Activated caspase-3 is induced in primary human myotubes that overexpress DOCK3. Three replicates in separate wells were used for both DOCK3 and vector controls. (**C**) Western blot images showing DOCK3 overexpression affects PTEN/AKT signaling levels. Western blot images of HA (DOCK3), PTEN, pAKT (S473 and T308), AKT (pan/recognizes all 3 AKT isoforms), PROCASPASE3 (top arrowhead), cleaved CASPASE-3 (bottom arrowhead), and a GAPDH loading control taken from 30 μg of protein whole-cell lysates overexpressing either the control empty vector or HA-DOCK3 in primary human myotubes. (**D**) TUNEL assay on DOCK3-overexpressing and control vector–overexpressing primary human myotubes. The TUNEL-positive nuclei (red) are costained with DAPI (blue) in the vector (pCI-HA) control– and HA-DOCK3–overexpressing samples. (**E**) The percentage of TUNEL-positive myonuclei in the vector control– or HA-DOCK3–overexpressing normal primary myotubes is shown on the graph. Two-hundred myonuclei were counted from at least 10 different fields for each condition. Three separate 2-well chamber slides were used in this experiment ($n = 6$ wells per condition). *$P < 0.005$. (**F**) DOCK3 overexpression fails to induce active RAC1 (RAC1-GTP) in normal and DMD primary myotubes overexpressing either HA-DOCK3 or a control vector. Western blot images of other RAC1 downstream signaling factors (CDC42 and RHOA), DOCK3, and a β-actin–loading control are also shown.

its expression is strongly induced in dystrophic muscle where miR-486 expression is significantly reduced.

DOCK3 overexpression induces myotube apoptosis and affects PTEN/AKT signaling. Previously, we demonstrated that inhibition of miR-486 expression resulted in increased apoptosis and decreased cellular migration following a scratch wound injury in human muscle cells (36). The increased levels of muscle cell apoptosis and poor cellular migration mimic findings reported for DMD muscle cells, with reduced cell proliferation and migration capabilities, in addition to an induction of caspase-mediated cell death (58–61). While there have been several studies showing that DOCK3 regulates cancer cell shape and migration via the RAC1/CDC42/RHOA signaling pathway, little is known about DOCK3 function in skeletal muscle (62, 63). Previous studies have shown that DOCK3 overexpression can regulate neuronal cell death in either positive or negative fashions, depending on the cell type and signaling pathways activated (64). To test DOCK3 function in skeletal muscle, we generated stable primary human myotube cell lines that overexpressed either full-length human DOCK3 or a vector control. DOCK3-overexpressing myoblasts were more elongated when compared with vector control myoblasts, but had no increased cell death (data not shown). Upon induction of myogenic differentiation via serum withdrawal, DOCK3-overexpressing human myotubes formed smaller, malformed mononuclear myotube aggregates when compared with

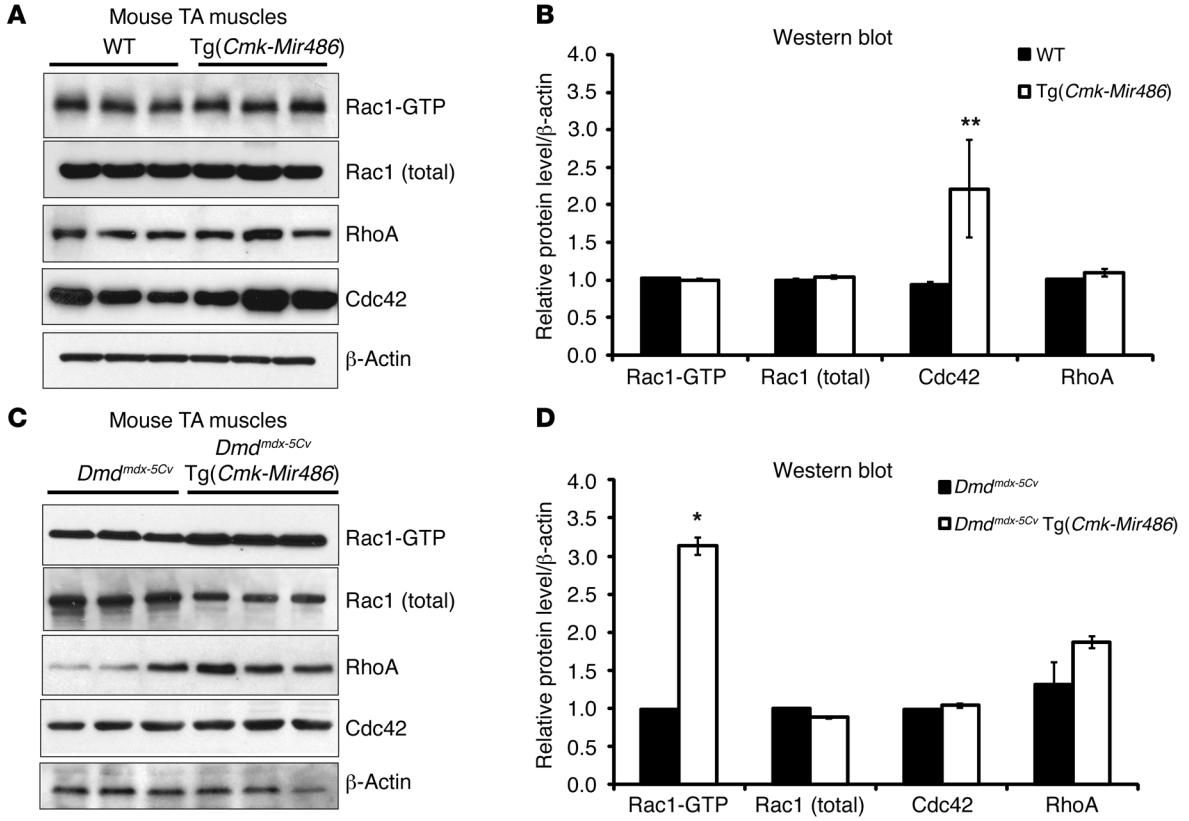

Figure 9

RAC1 activation is induced in miR-486–overexpressing muscles. (**A**–**D**) The overexpression of miR-486 in dystrophic *Dmd*$^{mdx\text{-}5Cv}$ muscles results in increased levels of active Rac1 (Rac1-GTP). (**A**) Western blot images of whole-tissue lysates from adult (2 to 4 months old) WT and Tg(*Cmk-Mir486*) mouse TA muscles. Three mice were used per genotype cohort. (**B**) Densitometry graph of the Western blot images of whole-tissue lysates from adult WT and Tg(*Cmk-Mir486*) mouse TA muscles. (**C**) Western blot images of whole-tissue lysates from adult (2 to 4 months old) *Dmd*$^{mdx\text{-}5Cv}$, and *Dmd*$^{mdx\text{-}5Cv}$ Tg(*Cmk-Mir486*) mouse TA muscles. (**D**) Densitometry graph of the Western blot images of whole-tissue lysates from adult WT and Tg(*Cmk-Mir486*) mouse TA muscles. Western blot protein levels were normalized to the total levels of the β-actin–loading control. *$P < 0.005$; **$P < 0.05$.

vector control myotubes (Figure 8A). DOCK3-overexpressing myotubes had higher expression of activated caspases-3/7 compared with controls, suggesting increased cell death (Figure 8B). Several studies have shown that PTEN/AKT signaling levels are linked to myotube growth and survivability (15, 16, 65). We next tested whether DOCK3 overexpression was linked to the expression levels of PTEN/AKT signaling factors. Overexpression of DOCK3 in myotubes resulted in decreased phosphorylated AKT (S473 and T308), with a corresponding increase in PTEN protein levels (Figure 8C). Additionally, we observed a significant increase in the levels of cleaved caspase-3 in the DOCK3-overexpressing myotubes, indicating the induction of cell death pathways. We next performed a TUNEL assay and quantified the number of TUNEL-positive myonuclei on DOCK3-overexpressing and control vector overexpressing primary myotubes. We observed a significant increase in the amount of TUNEL-positive nuclei in the DOCK3-overexpressing myotubes, further indicating that DOCK3 overexpression induces apoptosis (Figure 8, D and E). These results are consistent with our findings demonstrating that miR-486 overexpression has a cytoprotective effect in muscle via modulation of the PTEN/AKT signaling pathway and that DOCK3 levels also have an important function in the regulation of this pathway.

Overexpression of DOCK3 fails to activate RAC1 in dystrophin-deficient myotubes. DOCK3 has been shown to be an essential activator of the Rho-GTPase protein RAC1 by directly binding to RAC1 at the plasma membrane, thereby subsequently regulating cellular membrane spreading in an actin-dependent manner (66). RAC1 is a small GTPase protein and its active form (RAC1-GTP) has been shown to activate phosphorylated-AKT whilst modulating the several PTEN/AKT signaling components (67). The dystrophin-glycoprotein complex (DGC) is an essential docking point for RAC1 binding to dystroglycan and an essential interaction for RAC1 activation (68, 69). Previous studies have demonstrated that RAC1 activation of phosphorylated AKT is dependent on cellular membrane stability in that atrophied laminin-depleted and β-dystroglycan–depleted muscle RAC1 failed to activate AKT (70). We hypothesized that DOCK3 might similarly fail to activate RAC1 and subsequently affect the PTEN/AKT signaling pathway due to the lack of cellular membrane stability found in dystrophin-deficient muscle. We tested whether overexpression of DOCK3 was capable of increasing the levels of the active form of RAC1 in normal and DMD myotubes. As expected, overexpression of DOCK3 in normal human primary myotubes resulted in higher protein levels of activated RAC1 (RAC1-GTP) (Figure 8F). Con-

versely, overexpression of DOCK3 in DMD human primary myotubes resulted in no change in the levels of RAC1-GTP (Figure 8F). These findings suggest that DOCK3 cannot activate RAC1, possibly due to the cellular membrane instability caused by dystrophin deficiency. Recently, it has been shown that RAC1 activation is essential for normal myoblast fusion (71, 72). We next tested whether or not overexpression of miR-486 affected the amount of active RAC1 via RAC1-GTP immunoprecipitation assays in normal and DMD primary human myotubes. The overexpression of miR-486 resulted in no significant change in the amounts of active RAC1 in normal myotubes (Supplemental Figure 6). However, we observed significantly increased levels of RAC1 in miR-486–overexpressing DMD myotubes (Supplemental Figure 6). These findings suggest that RAC1 activation is induced by miR-486 overexpression, which had failed to occur when DOCK3 was overexpressed in DMD myotubes. Given that miR-486 overexpression seems to delay the myofiber membrane instability resulting from the lack of dystrophin, we measured the levels of active Rac1 via immunoprecipitation assays in Tg(*Cmk-Mir486*) mice on normal and $Dmd^{mdx\text{-}5Cv}$ backgrounds. In Tg(*Cmk-Mir486*) mice under normal background, we observed no change in the levels of active Rac1 compared with WT littermate controls (Figure 9, A and B). This finding implies that, despite the reduction of DOCK3 protein, activated Rac1 can still function normally in skeletal muscle. Other Rac1 downstream signaling factors were also not significantly altered by miR-486 overexpression, with the exception of Cdc42 (Figure 9, A and B). In contrast, we detected significantly higher levels of active Rac1 in the $Dmd^{mdx\text{-}5Cv}$ Tg(*Cmk-Mir486*) mice when compared directly to $Dmd^{mdx\text{-}5Cv}$ littermates (Figure 9, C and D). This suggests that the increase in sarcolemma stability resulting from miR-486 muscle overexpression facilitates the remaining Dock3 (or other GTPases) to activate Rac1 and, subsequently, other downstream signaling factors. Our overall findings demonstrate that miR-486 overexpression in skeletal muscle can delay or prevent many of the histological, biochemical, and physiological deficits associated with dystrophin deficiency in mice.

Discussion

The overexpression of miR-486 transcript appears to have profound beneficial effects in ameliorating the disease progression in dystrophic skeletal muscle. miR-486 overexpression in dystrophic mouse skeletal muscle prevents the degeneration of the muscle myofiber membranes that is often associated with the disease. We have demonstrated that DOCK3 is a target of miR-486 and that overexpression of miR-486 suppresses DOCK3 expression while increasing the levels of phosphorylated AKT. Furthermore, we demonstrate that overexpressed DOCK3 cannot activate its downstream target RAC1 (an activator of PTEN/AKT signaling in normal muscle) in dystrophin-deficient muscle. Additionally, we demonstrate that the overexpression of miR-486 in dystrophin-deficient human myotubes and $Dmd^{mdx\text{-}5Cv}$ mice is able to restore RAC1 activity and potentially block the cell death that occurs in DMD disease pathology.

miR-486 as a modulator of PTEN/AKT signaling in skeletal muscle. In our present study, we identified miR-486 as a potent regulator of PTEN/AKT signaling in skeletal muscle in a dystrophic mouse model. These findings complement our previous findings in which we overexpressed miR-486 in primary human myoblasts and demonstrated that miR-486 directly inhibits PTEN protein levels while inversely inducing the levels of phosphorylated AKT (36). These findings are consistent with 2 other studies that demonstrated that miR-486 overexpression could directly inhibit PTEN protein levels in rat cardiomyocytes or when injected as an oligo mimic directly into the skeletal muscle (37, 55). The function of PTEN in skeletal muscle is independent and distinct of its well-described role as a tumor-suppressor gene (73). Deletion of *Pten* in skeletal myofibers resulted in improved muscle regeneration in mice fed a high-fat diet (22). Genetic deletion of *Pten* in the *Myf5* lineage resulted in mice having increased body weights due to a shift in the tissue distribution of white fat adipocyte progenitors (74). These results are in agreement with our previously described studies in Tg(*Cmk-Mir486*) mice, which showed significant increases in fat pad, but not muscle weight, due to a reduction of *Pten* levels in the myofiber (36). Indeed, it has been recently demonstrated that human patients with a *PTEN* haploinsufficiency have increased insulin sensitivity, obesity, and elevated phosphorylated-AKT levels in their adipose tissue (75). Additionally, by reducing *Pten* levels in dystrophic mouse muscle due to miR-486 overexpression, phosphorylated *Akt* levels significantly increased. Previous studies have shown that overexpression of the constitutively active myristoylated form of *Akt* (myr-*Akt*) induces muscle hypertrophy both in vitro and in vivo and offers protective effects against muscle degeneration and damage in the Dmd^{mdx} strain (10, 17, 20).

DOCK3 is an essential regulator of PTEN/AKT and RAC1 signaling in normal and dystrophic muscle. In the present study, we demonstrate that DOCK3 is a direct target of miR-486 in both normal and dystrophic muscle. DOCK3 has been shown to be an essential regulator of cell movement and apoptosis via the modulation of RAC1 signaling by converting RAC1-GDP into RAC1-GTP via DOCK3's GTPase activity (66, 76). Normal cellular migration and viability are significantly affected if DOCK3 is overexpressed or silenced, depending on the cell type (62, 64). *Dock3*-deficient mice have axonal degeneration, and a family carrying mutations resulting in nonfunctional DOCK3 protein have been linked to attention deficit hyperactivity disorder–like phenotype (77, 78). DOCK3 protein expression levels are thought to be regulated by let-7i in a process that has been shown to be essential for RAC1 activation in cancer cells (63). The entire RAC1/CDC42/RHOA signaling pathway is an essential regulator of normal myoblast fusion (71, 79, 80).

Here, we demonstrate that DOCK3 overexpression fails to activate RAC1 in DMD myotubes, but this can be corrected by the overexpression of miR-486. Previous studies have shown that the activation of RAC1 is impaired if the DGC complex is disrupted in atrophied or sarcoglycan-defective muscle (70). However, we also show that miR-486 represses DOCK3 protein levels in muscle, but still results in increased activated RAC1 levels. This finding may be due to the fact that other DOCK family proteins (such as DOCK1) or other muscle proteins are capable of activating RAC1 (such as Def6 or Parvb) as a means of compensating for the decreased levels of DOCK3 resulting from miR-486 overexpression (81–83). Interestingly, the DOCK family of proteins has recently been shown to directly bind to phosphoinositides, which are well-characterized regulators of PTEN/AKT signaling (84). It is possible that miR-486 suppression of DOCK3 protein levels directly alters PTEN/AKT signaling independently of RAC1/CDC42/RHOA signaling in dystrophic muscle.

MicroRNA overexpression as a therapy for muscle disease. As the technologies for identifying and functionally characterizing microRNAs improve, opportunities to modulate their expression levels for therapeutic benefit in various disease states emerge. Previously, we and

others have profiled dysregulated microRNAs from 3 dystrophin-deficient species (human, mouse, and zebrafish), and identified common microRNAs with a unique biosignature for the diseased state (35, 85, 86). Profiling of several of these microRNAs, including the muscle-enriched miR-1, miR-133a, and miR-206, have been shown as useful serum biomarkers in dystrophic mice (87). The dynamic functional roles *Pten* plays in muscle growth and physiology are mirrored by the regulation of *Pten* expression levels by a variety of microRNAs (73, 88, 89). MicroRNAs regulate critical aspects of myogenic processes, including myogenic cell proliferation, differentiation, muscle performance, and cell fusion (34, 90–92). One class of microRNAs is embedded within 3 separate myosin heavy chain loci, miR-208a (Myh6), miR-208b (Myh7), and miR-499a (Myh7b), and all 3 microRNAs regulate myofiber type (fast, slow, or mixed) and identity (90). Another class of muscle microRNAs is directly regulated in expression levels by the transcriptional activity of the serum response factor (SRF) gene (93, 94). Additionally, several microRNAs are either directly or indirectly related to muscle disease or the progression of a myopathic phenotype (85, 95, 96). For example, miR-133a downregulates dynamin-2, a GTPase protein that is deficient in humans with centronuclear myopathy (96, 97).

Direct modulation of microRNA expression levels might also serve as a means of modulating muscle disease pathologies. Direct inhibition of the fibrosis-induced microRNA miR-21 has been proposed to enhance TGF-β's proliferative effects on dystrophic muscle, enhance AKT signaling, and thereby promote muscle regeneration in Dmd^{mdx} muscles (39). Similarly, loss of miR-29 expression in dystrophic mouse muscle is thought to induce the TGF-β–dependent fibrotic response in Dmd^{mdx} mice (98). Recently, it has been shown that miR-206 expression levels are essential for normal skeletal muscle regeneration and myogenic fusion (99). Genomic ablation of miR-206 in Dmd^{mdx} mice resulted in severe degeneration of muscle fibers, and expression of miR-206 was essential for delaying the progression of the dystrophin-deficient disease pathology in mice (99). Given that miR-206 and miR-486 seem to have somewhat similar expression patterns in muscle, one might speculate that genomic ablation of miR-486 in Dmd^{mdx} mice might have a similar effect in worsening the dystrophic disease pathology (38). In parallel studies, transient electroporation of miR-486 mimics boosted muscle regeneration in the chronic-kidney disease (CKD) muscle-wasting mouse model by directly inhibiting Foxo1 expression and simultaneously blocking *Pten* expression (55). More recently, another group has shown that miR-486 is a direct target of myostatin signaling, and that genetic ablation of myostatin induces myotube hypertrophy via miR-486 and PTEN/AKT signaling (100). Several groups have shown that overexpression of muscle microRNAs can ameliorate some pathological signs of muscle disease in murine models (101, 102). One can envision that miR-486 overexpression via adeno-associated virus (AAV) might have beneficial effects on dystrophin-defective muscles by promoting muscle hypertrophy and promoting regeneration (103). Thus, the overexpression of some of these muscle-enriched microRNAs might offer another therapeutic entry point for delaying or ameliorating the progression of the disease pathology of muscular dystrophy.

Methods

MicroRNA extraction and expression profiling. MicroRNA obtained from a commercially available adult human tissue panel (FirstChoice HumanTotal RNA Survey Panel; Ambion) was used to profile miR-486-5p transcript levels. For mice, adult male mice (2 to 4 months) were used to determine miR-486-5p transcript levels in multiple tissues. Three replicates were used for human and mouse tissues, and expression levels were normalized to both the thymus and an RNU6-2 loading control. MicroRNA was extracted using the miRVana kit (Ambion) following the manufacturer's protocol.

Mice. The Tg(*Cmk-Mir486*) (MCK–Tg[*Cmk-Mir486*]) transgenic mice were maintained on at C57BL6/J background (Jackson Laboratories) and originally described elsewhere (36). The $Dmd^{mdx\text{-}5Cv}$ mouse strain was originally purchased from the Jackson Laboratory and maintained on a C57BL6/J background for over 6 generations (27). $Dmd^{mdx\text{-}5Cv}$ mice were genotyped for the detection of the A-to-T transversion at exon 10 of the mouse Dystrophin gene using a modified version of primer competition PCR genotyping protocol previously described (104). The primers used in the reaction were the following: WT: 5′-GATACGCTGCTTTAATGCCTTTACTTCTTCAA-CATCATTTGAAATCTCT-3′, $Dmd^{mdx\text{-}5Cv}$: 5′-CGGCCACTTCTTCAA-CATCATTTGAAATCTCA-3′, and combined: 5′-GCGCGACGGAAG-TAAATCTGGATAGTTACCAA-3′ along with GoTaq DNA polymerase (Promega; M3001) and Flexi Buffer (Promega; M8901). Approximately 0.2 mM dNTPs, 2 mM MgCl2 (Promega; A3511), and all 3 genotyping primers (1 μM final concentration) were used in a 20 μl reaction. The WT PCR amplicon was 143 base pairs, while the $Dmd^{mdx\text{-}5Cv}$ mutant PCR amplicon was 126 base pairs. The $Dmd^{mdx\text{-}5Cv}$ Tg(*Cmk-Mir486*) mice (also on a C57BL6/J background) were generated by mating male Tg(*Cmk-Mir486*) mice on a WT C57BL6/J background with $Dmd^{mdx\text{-}5Cv}$ homozygous females. The $Dmd^{mdx\text{-}5Cv}$ Tg(*Cmk-Mir486*) males were subsequently bred to $Dmd^{mdx\text{-}5Cv}$ homozygous females, and the $Dmd^{mdx\text{-}5Cv}$ offspring from that mating that lacked the miR-486 transgene served as littermate controls. All animals were housed in sterile, pathogen-free isolation cages.

Cardiotoxin injury. As described previously, mice were injured using an injection of 40 μl of 10 μM cardiotoxin isolated from *Naja mossambica mossambica* snake venom (Sigma-Aldrich, C-9759) into the right TA muscle (36). The left, contralateral TA muscle served as an uninjured control.

Treadmill assay. Mice were run on an Exer-3/6 treadmill (Columbus Instruments) set at a 10-degree downhill decline. Mice were warmed up at a speed of 5 m/min for 5 minutes prior to the experimental test. During the test phase, mice were run at a speed of 5 m/min for 2 minutes, 7 m/min for 2 minutes, 8 m/min for 2 minutes, and 10 m/min for 5 minutes. The treadmill speed was then increased at a rate of 1 m/min to a final speed of 20 m/min. Mouse exhaustion was defined by the inability of the mouse to remain on the treadmill despite electrical prodding set at a current of 0.6 mAmps. The electrical prodding was turned off if the mouse showed no movement toward the treadmill track after 5 seconds of motionlessness.

Mouse activity assays. The mouse 6-minute activity assays were performed following a protocol previously described, with slight modifications (45, 46). The mice were run for 5 minutes at 3 m/min, followed by an increase to 10 m/min for 10 minutes. Pre- and posttreadmill activity (total distance and vertical activity) were measured for 6 minutes using ActiTrack v2.7 software (Panlab). Five adult (2 to 4 months old) mice of each of the 4 genotype cohorts were used in all experiments.

Cage-grip strength and wire hang assays. Mouse forelimb grip strength was measured on a metal cage-grip strength transducer (Columbus Instruments) and calculated as maximum force output by a Chatillon grip strength meter (AMETEK Inc.). The maximum forelimb force output after 5 separate attempts was normalized to the mouse body weight in kilograms. Five mice per genotype cohort were used for experimental analysis. For the wire-hang assays, mice had to grasp a securely suspended metal cage with their forelimbs. Time was measured from the initial grasp until their fall onto a bottom cage lined with soft bedding. Mice were measured 3 separate times with a 10-minute rest interval between attempts. The average time to fall was recorded for analysis. Five mice per genotype cohort were used for experimental analysis.

EBD assays and immunofluorescence of tissue sections. Mice underwent i.p. injections with 10 mg/ml of EBD (Sigma-Aldrich; E-2129) at a dosage of 100 μl per 10 g of total body weight approximately 24 hours prior to the treadmill assay. Mouse muscles were harvested immediately following the treadmill assay and snap frozen in isopentane cooled in liquid nitrogen. Then 600 laminin-α2 positively stained myofibers were counted for the inclusion of the EBD. For this experiment, 3 mice of each of the 4 genotype cohorts were used. Mouse sections were cryoembedded in Tissue-Tek OCT medium and were sectioned on a cryostat at a thickness of 7 microns and placed on permafrosted slides. Tissue sections were fixed in either 4% paraformaldehyde (Electron Microscopy Sciences) or absolute methanol (Sigma-Aldrich) for 10 minutes at 4°C. The samples were then blocked and incubated with primary antibody overnight following the manufacturer's protocol and using reagents from the MOM Basic Kit (Vector Labs). A secondary antibody (anti-rat Alexa Fluor 568) was used for immunofluorescent detection of primary antisera. Slides were then washed 3 times with 0.1% Triton-X 100/1× PBS before being mounted with Vectashield containing DAPI (Vector Labs). Slides were imaged with a Nikon II microscope (Nikon Instruments Inc.) using OpenLab software version 3.1.5 (Improvision/PerkinElmer). Images were later modified in Adobe Photoshop version CS4 (Adobe Systems Inc.) for clarity and resolution.

Muscle fiber type immunofluorescence and analysis. Skeletal muscle sections were obtained from the gastrocnemius, soleus, and TA muscles of adult male mice from the 4 genotype cohorts, fixed in 100% acetone for 5 minutes at room temperature, then air dried for 20 minutes. A commercial kit (MOM, FMK-2201; Vector Labs) was used to reduce nonspecific antibody binding. Muscle sections were then stained with monoclonal antibodies to detect type I (slow, BA-F8), type IIa (fast, SC-71), and type IIb (fast, BF-F3) myosin heavy chain following a standard immunofluorescence protocol (50). Then 600 TA, 600 gastrocnemius, and 200 soleus muscle fiber types were counted and quantified in 3 mice per genotype cohort (n = 3 mice). Slides were imaged with a Zeiss LSM 700 Laser Scanning Confocal at ×10 objective, and Zen software (Carl Zeiss Microscopy, LLC) was used for image capture. ImageJ (NIH) was used to generate montages of muscle sections for fiber counting. Photoshop version CS4 (Adobe Systems Inc.) was used to adjust resolution and contrast for representative images. A Mann-Whitney U test was used to calculate values of significance amongst the 4 genotype cohorts.

Serum biochemical measurements. Serum from adult (2 to 4 month old) and aged (10 to 14 months old) mice was obtained by tail-vein bleeds and collected into capillary tubes. Whole serum (approximately 40 μl per mouse bleed) was spotted on assay chips and analyzed on the VetScan VS2 (Abaxis) analyzer by the Animal Resources at Boston Children's Hospital core facility to measure ALT enzymatic levels. Serum CK assays were performed using the Pointe Scientific Inc. CK kit with serum standards purchased from Stanbio Laboratory. All mice used were age-matched and littermates, unless otherwise stated. Each assay was run at n = 5 mice per mouse genotype cohort.

Muscle physiology experiments. Mice were anesthetized with sodium pentobarbital (i.p. injection of 80 mg/kg) for limb, muscle, and diaphragm removal (euthanasia via pneumothorax). The EDL, soleus, and a narrow strip dissected from the diaphragm were maintained ex vivo in a bicarbonate buffer (35°C, equilibrated with 95% O_2, 5% CO_2) and assayed for tetanic force per muscle physiological CSA (specific force) as previously described (105, 106). A minimum of 8 mice (WT and *Dmd*$^{mdx\text{-}5Cv}$) and a maximum of 12 (Tg[*Cmk-Mir486*] and *Dmd*$^{mdx\text{-}5Cv}$ Tg[*Cmk-Mir486*]) were used per genotype cohort, from only males of both the adult (2 to 4 month old) and old (10 to 14 months old) ages. Only tetanic force measurements from male mice are shown; however, we observed no significant differences in the increase in tetanic force output in female *Dmd*$^{mdx\text{-}5Cv}$ Tg(*Cmk-Mir486*) when compared with their *Dmd*$^{mdx\text{-}5Cv}$ female littermate controls (data not shown). All of the data were analyzed by 1-way ANOVA followed by evaluation of significant treatment effects with Tukey"s HSD post hoc test. The type I error rate was set at $P < 0.05$.

Human myoblast cell lines. Normal and DMD human myoblast cell lines derived from patient muscle biopsies were isolated and cultured as previously described (36). To establish the stable myoblast cell lines that overexpressed either HA-DOCK3 or pCI-Neo (Promega) constructs, 4 μg of plasmid was electroporated into human unaffected or DMD low-passaged primary myoblasts using the Amaxa Cell Line Nucleofector Kit V (Lonza). Forty-eight hours after electroporation, the positively electroporated cells were selected using gentamicin sulfate (400 μg/ml; RPI Corp). Stable cell lines were maintained with medium containing a gentamicin sulfate at a concentration of 200 μg/ml. Three separate stable lines of each construct were generated. The human pCI-HA-DOCK3 overexpression plasmid was a gift from Hideo Kimura (Department of Molecular Genetics, National Institute of Neuroscience, National Center of Neurology and Psychiatry, Kodaira, Tokyo, Japan) and has been described elsewhere (66).

Histochemical analysis. Mouse muscle tissues were cryoembedded in Tissue-Tek OCT medium (Sakura Finetek USA, Inc.) in an isopentane (Sigma-Aldrich) liquid nitrogen bath. Muscles were sectioned on a cryostat at a thickness of 7 μm and placed on permafrosted slides (VWR Scientific). H&E (Sigma-Aldrich) staining was performed as previously described (36). 600 TA and gastrocnemius myofibers from at least 5 separate fields were counted for determining CSA and centralized myonuclei values for each of the 4 genotype cohorts (n = 3 mice per genotype cohort); 200 diaphragm myofibers from at least 5 separate fields were counted for determining CSA and centralized myonuclei values for each of the 4 genotype cohorts (n = 3 mice per genotype cohort). CSAs of TA muscle fibers were calculated from at least 10 separate fields that contained at least 600 individual, nonconsecutive fibers that had been stained with H&E. Average CSA was then determined using SPOT imaging software. At least 3 (n = 3) mice were used per cohort.

Lentivirus constructs. Lentiviruses were produced in HEK293T (GenHunter) grown in 10% FBS/DMEM and supplemented with antibiotics. The lentiviruses were transduced into human muscle cells with polybrene (8 μg/ml; Sigma-Aldrich) as previously described (36). miR-486 overexpression lentivirus was obtained commercially (System Biosciences Inc.).

Plasmids. The microRNA 3′ UTR luciferase reporter plasmids that contained the miR-486–binding sites were generated by PCR amplification of an existing human DOCK3 3′ UTR clone (SwitchGear Genomics) with Spe1 and Not1 restriction sites added to the DNA ends. Three critical miR-486 seed site nucleotides were mutated from G**T**A**C**A**G**GA to GgAaAtGA using site-directed mutagenesis to generate the human DOCK3 3′ UTR luciferase reporter mutant construct as previously described (boldface text indicates where mutations to the miR-486 seed sequences were made; lowercase letters indicate the exact mutations made) (36). The microRNA reporter assays were performed as previously described (36).

Western blot analysis. Protein lysates from tissues were homogenized using a FastPrep FP120 (Thermo Fisher Scientific Inc.) column homogenizer within Lysing Matrix D columns (MP Biomedicals) in T-PER buffer (Thermo Fisher Scientific Inc.). Proteins were extracted from cells using M-PER buffer (Thermo Fisher Scientific Inc.), and samples were directly lysed on the plate. All lysis buffers contained Mini EDTA-Free Protease Inhibitor Tablets (Roche Applied Sciences), and some lysis buffers were supplemented with PhosSTOP Phosphotase Inhibitor Cocktail Tablets (Roche Applied Sciences). Protein was quantified using a Pierce BCA Protein Assay Kit (Thermo Fisher Scientific Inc.). Approximately 30 μg of total tissue protein lysate or 25 μg of total cell lysate were electrophoretically resolved on 4% to 20% Novex (Life Technologies) gradient gels. The proteins were transferred to PVDF membranes (Life Technologies), blocked with 3% BSA

(RPI Corp.) diluted in 0.1% TBS-Tween or 5% nonfat milk diluted in 0.1% TBS-Tween for 1 hour before being incubated in primary antisera overnight at 4°C with gentle agitation. Blots were washed in 0.1% TBS-Tween 3 times for 5-minute intervals before being incubated with secondary antisera (mouse or rabbit) conjugated to HRP for 1 hour at room temperature with gentle agitation. Following another 3 washes for 15-minute intervals at room temperature, membranes were then treated with RapidStep ECL Reagent (Calbiochem) and exposed to x-ray film (Genesee Scientific). Some Western blot images were acquired using a Typhoon Variable Mode Imager (Amersham Pharmacia). Some membranes were stripped using Restore Plus Western Blot Stripping Buffer (ThermoScientific) and later probed with different antisera. Western blot densitometry was performed using open-source ImageJ software.

Rac1 immunoprecipitation/activity assays. Rac1-GTP and total Rac1 expression levels were measured using the Active Rac1 Pull-Down and Detection Kit (Thermo Fisher Scientific Inc.) following the manufacturer's protocol. Twenty-five micrograms of whole-cell lysates were used to determine the Rac1-GTP levels in the human myotube cell cultures. One-hundred micrograms of total protein tissue lysates were used in the Rac1-GTP immunoprecipitation assay to determine the Rac1-GTP levels in the TA muscles of the adult WT, Tg(*Cmk-Mir486*), $Dmd^{mdx\text{-}5Cv}$, and $Dmd^{mdx\text{-}5Cv}$ Tg(*Cmk-Mir486*) mice (2- to 6-month-old male mice; $n = 3$ mice per genotype). Twenty-five micrograms of the total protein lysate inputs from cell and muscle lysates were used as a normalization control to measure the levels of total Rac1 protein and a β-actin loading control.

TUNEL assays. TUNEL assays were performed on DOCK3-overexpressing or control vector–overexpressing primary myotubes using a TACS 2 TdT-Fluor In Situ Apoptosis Kit (Trevigen) following the manufacturer's protocol. Briefly, myotubes grown in 0.1% gelatin-coated (Sigma-Aldrich) 2-well plastic chamber slides were fixed in 4% paraformaldehyde for 10 minutes at 4°C and underwent a series of 1× PBS washes in glass Coplin jars. Following an incubation with proteinase K and an additional 2 washes in deionized water, the slides underwent a 1-hour labeling reaction while being incubated at 37°C in a humidity chamber. The reaction was then stopped with the 1× TdT Stop Buffer from the kit, and the slides were washed an additional 2 times in deionized water. The slides were then incubated in the kit's Strep-Fluor solution for 20 minutes at room temperature and then were washed an additional 2 times in deionized water. The slides were air-dried before being placed in the dark prior to imaging on a Nikon II microscope using OpenLab software version 3.1.5. Two-hundred DAPI-positive nuclei from 10 separate fields were counted ($n = 3$ separate slides for each condition).

Antisera. A list of all primary antisera and the dilutions used in this manuscript can be found in Supplemental Table 1.

Real-time quantitative PCR. MicroRNA and total RNA were extracted from either cell lines or mouse/human muscle biopsies using a miRVana Isolation Kit (Ambion). Fifty nanograms of total miRNA per sample were reverse transcribed into cDNA using the Multiscribe RT System (Applied Biosystems), and 1 μl of RT reaction was used for each specific microRNA TaqMan assay (Applied Biosystems). The microRNA was then amplified using NoAmp Erase TaqMan Polymerase (Applied Biosystems) following the manufacturer's instructions. MicroRNA TaqMan assays (Applied Biosystems) were run using a TaqMan Universal Master Mix Kit (Applied Biosystems) following the manufacturer's instructions. All samples were analyzed in 96-well optical plates on an ABI 7900HT Real-Time PCR Machine (Applied Biosystems). Cycle times were normalized to U6 snRNA as a loading control. Relative fold expression and changes were calculated using the $2^{-\Delta\Delta Ct}$ method (107).

For all SYBR green–based real-time quantitative PCR assays, total RNA from muscle biopsies and cell cultures was extracted using the mirVana miRNA/mRNA Extraction Kit (Ambion). One microgram of total RNA was copied into cDNA using the First-Strand Synthesis Kit (Invitrogen). Ten-fold serial dilutions of the cDNA were analyzed on 96-well optical plates using the Power SYBR Green Mix System (Applied Biosystems) and analyzed on the ABI 7900HT Real-Time PCR Machine (Applied Biosystems). Primers specific for each gene were designed using NCBI-PrimerBlast, and all cycle time values were normalized to an 18sRb loading control. A list of SYBR green–based real-time PCR primers can be found in Supplemental Table 2.

Statistics. Unless otherwise stated, all statistical analysis was performed using Student's *t* test (2-tailed). All muscle-force experiments were analyzed with 1-way ANOVA followed by Holm-Sidak's multiple comparison test.

Study approval. All animal studies were approved by the Boston Children's Hospital Animal Resources at Children's Hospital (ARCH) Review Board (protocol number 12-10-2287R). All patients and/or their guardians gave written and oral consent prior to surgery, and all protocols were approved by the Boston Children's Hospital Human Subjects Internal Review Board (protocol number: 03-12-205R).

Acknowledgments

Funding for this work was generously provided by the Bernard F. and Alva B. Gimbel Foundation (to L.M. Kunkel) and through NIH grant P50 NS040828-10. Research reported in this publication was supported by the National Institute of Arthritis and Musculoskeletal and Skin Diseases of the NIH under award number R01AR064300 (to L.M. Kunkel). P.B. Kang is supported by the Muscular Dystrophy Association (MDA) (MDA186796) and NIH grant R01 NS080929. M.S. Alexander is supported by an MDA development grant (MDA255059). F. Rahimov is supported by an MDA development grant (MDA202863). Activity and treadmill experiments were performed with equipment provided by the Boston Children's Hospital Intellectual and Developmental Disabilities Research Center (IDDRC) Neurodevelopmental Behavioral Core facilities, which is supported by an NIH grant (CHB IDDRC P30-HD18655). The MF20 (myosin heavy chain) antibody was developed by the laboratory of D.A. Fischman. The BA-F8, SC-71, and BF-F3 myosin antibodies were developed by S. Schiaffino and were all obtained from the Developmental Studies Hybridoma Bank developed under the auspices of the National Institute of Child Health and Development (NICHD) and maintained by The University of Iowa, Department of Biology, Iowa City, Iowa, USA. We are grateful for the critical evaluation of this manuscript by members of the Kunkel Lab, Hart Lidov, and Emanuela Gussoni. Finally, we wish to thank the families and patients who donated the muscle biopsies that we used in this study.

Received for publication October 4, 2013, and accepted in revised form March 20, 2014.

Address correspondence to: Louis M. Kunkel, Boston Children's Hospital, 3 Blackfan Circle CLS15027.3, Boston, Massachusetts 02115, USA. Phone: 617.355.6729; Fax: 617.730.0253; E-mail: kunkel@enders.tch.harvard.edu.

Peter B. Kang's present address is: Division of Pediatric Neurology, University of Florida College of Medicine, Gainesville, Florida, USA.

1. Emery AE. The muscular dystrophies. *Lancet*. 2002;359(9307):687–695.
2. Goemans NM, et al. Systemic administration of PRO051 in Duchenne's muscular dystrophy. *N Engl J Med*. 2011;364(16):1513–1522.
3. Cirak S, et al. Exon skipping and dystrophin restoration in patients with Duchenne muscular dystrophy after systemic phosphorodiamidate morpholino oligomer treatment: an open-label, phase 2, dose-escalation study. *Lancet*. 2011;378(9791):595–605.
4. Liew WK, Kang PB. Recent developments in the treatment of Duchenne muscular dystrophy and

spinal muscular atrophy. *Ther Adv Neurol Disord*. 2013;6(3):147–160.
5. Mendell J, et al. Eteplirsen for the treatment of duchenne muscular dystrophy. *Ann Neurol*. 2013; 74(5):637–647.
6. Lu Q-L, Yokota T, Garcia L, Muntoni F, Partridge T. The status of exon skipping as a therapeutic approach to duchenne muscular dystrophy. *Mol Ther*. 2011;19(1):9–15.
7. Ahmad A, Brinson M, Hodges BL, Chamberlain JS, Amalfitano A. Mdx mice inducibly expressing dystrophin provide insights into the potential of gene therapy for Duchenne muscular dystrophy. *Hum Mol Genet*. 2000;9(17):2507–2515.
8. Welch EM, et al. PTC124 targets genetic disorders caused by nonsense mutations. *Nature*. 2007; 447(7140):87–91.
9. Peter AK, et al. Myogenic Akt signaling upregulates the utrophin-glycoprotein complex and promotes sarcolemma stability in muscular dystrophy. *Hum Mol Genet*. 2009;18(2):318–327.
10. Kim MH, et al. Myogenic Akt signaling attenuates muscular degeneration, promotes myofiber regeneration and improves muscle function in dystrophin-deficient mdx mice. *Hum Mol Genet*. 2011; 20(7):1324–1338.
11. Marshall JL, et al. Sarcospan-dependent Akt activation is required for utrophin expression and muscle regeneration. *J Cell Biol*. 2012;197(7):1009–1027.
12. Haslett JN, et al. Gene expression comparison of biopsies from Duchenne muscular dystrophy (DMD) and normal skeletal muscle. *Proc Natl Acad Sci U S A*. 2002;99(23):15000–15005.
13. Haslett J, et al. The influence of muscle type and dystrophin deficiency on murine expression profiles. *Mamm Genome*. 2005;16(10):739–748.
14. Feron M, et al. PTEN contributes to profound PI3K/Akt signaling pathway deregulation in dystrophin-deficient dog muscle. *Am J Pathol*. 2009; 174(4):1459–1470.
15. Rommel C, et al. Mediation of IGF-1-induced skeletal myotube hypertrophy by PI(3)K/Akt/mTOR and PI(3)K/Akt/GSK3 pathways. *Nat Cell Biol*. 2001; 3(11):1009–1013.
16. Bodine SC, et al. Akt/mTOR pathway is a crucial regulator of skeletal muscle hypertrophy and can prevent muscle atrophy in vivo. *Nat Cell Biol*. 2001; 3(11):1014–1019.
17. Lai K-MV, et al. Conditional activation of Akt in adult skeletal muscle induces rapid hypertrophy. *Mol Cell Biol*. 2004;24(21):9295–9304.
18. Garcia-Cao I, et al. Systemic elevation of PTEN induces a tumor-suppressive metabolic state. *Cell*. 2012;149(1):49–62.
19. Ortega-Molina A, et al. Pten positively regulates brown adipose function, energy expenditure, and longevity. *Cell Metab*. 2012;15(3):382–394.
20. Blaauw B, et al. Akt activation prevents the force drop induced by eccentric contractions in dystrophin-deficient skeletal muscle. *Hum Mol Genet*. 2008; 17(23):3686–3696.
21. Majmundar AJ, et al. O_2 regulates skeletal muscle progenitor differentiation through phosphatidylinositol 3-Kinase/AKT signaling. *Mol Cell Biol*. 2012;32(1):36–49.
22. Hu Z, et al. PTEN inhibition improves muscle regeneration in mice fed a high-fat diet. *Diabetes*. 2010; 59(6):1312–1320.
23. Kunkel LM, Bachrach E, Bennett RR, Guyon J, Steffen L. Diagnosis and cell-based therapy for Duchenne muscular dystrophy in humans, mice, and zebrafish. *J Hum Genet*. 2006;51(5):397–406.
24. Bulfield G, Siller WG, Wight PA, Moore KJ. X chromosome-linked muscular dystrophy (mdx) in the mouse. *Proc Natl Acad Sci U S A*. 1984;81(4):1189–1192.
25. Sicinski P, Geng Y, Ryder-Cook AS, Barnard EA, Darlison MG, Barnard PJ. The molecular basis of muscular dystrophy in the mdx mouse: a point mutation. *Science*. 1989;244(4912):1578–1580.
26. Stedman HH, et al. The mdx mouse diaphragm reproduces the degenerative changes of Duchenne muscular dystrophy. *Nature*. 1991;352(6335):536–539.
27. Chapman VM, Miller DR, Armstrong D, Caskey CT. Recovery of induced mutations for X chromosome-linked muscular dystrophy in mice. *Proc Natl Acad Sci U S A*. 1989;86(4):1292–1296.
28. Danko I, Chapman V, Wolff JA. The frequency of revertants in mdx mouse genetic models for duchenne muscular dystrophy. *Pediatr Res*. 1992; 32(1):128–131.
29. Beastrom N, et al. mdx(^{5}cv) mice manifest more severe muscle dysfunction and diaphragm force deficits than do mdx mice. *Am J Pathol*. 2011; 179(5):2464–2474.
30. Bartel DP. MicroRNAs: target recognition and regulatory functions. *Cell*. 2009;136(2):215–233.
31. Grimson A, Farh KK-H, Johnston WK, Garrett-Engele P, Lim LP, Bartel DP. MicroRNA targeting specificity in mammals: determinants beyond seed pairing. *Mol Cell*. 2007;27(1):91–105.
32. Friedman RC, Farh KK-H, Burge CB, Bartel DP. Most mammalian mRNAs are conserved targets of microRNAs. *Genome Res*. 2009;19(1):92–105.
33. van Rooij E, Olson EN. MicroRNAs: powerful new regulators of heart disease and provocative therapeutic targets. *J Clin Invest*. 2007;117(9):2369–2376.
34. Williams AH, Liu N, van Rooij E, Olson EN. MicroRNA control of muscle development and disease. *Curr Opin Cell Biol*. 2009;21(3):461–469.
35. Eisenberg I, et al. Distinctive patterns of microRNA expression in primary muscular disorders. *Proc Natl Acad Sci U S A*. 2007;104(43):17016–17021.
36. Alexander M, et al. Regulation of DMD pathology by an ankyrin-encoded miRNA. *Skeletal Muscle*. 2011;1:27.
37. Small EM, et al. Regulation of PI3-kinase/Akt signaling by muscle-enriched microRNA-486. *Proc Natl Acad Sci U S A*. 2010;107(9):4218–4223.
38. Dey BK, Gagan J, Dutta A. miR-206 and -486 induce myoblast differentiation by downregulating Pax7. *Mol Cell Biol*. 2011;31(1):203–214.
39. Ardite E, Perdiguero E, Vidal B, Gutarra S, Serrano AL, Muñoz-Cánoves P. PAI-1-regulated miR-21 defines a novel age-associated fibrogenic pathway in muscular dystrophy. *J Cell Biol*. 2012; 196(1):163–175.
40. Straub V, Rafael JA, Chamberlain JS, Campbell KP. Animal models for muscular dystrophy show different patterns of sarcolemmal disruption. *J Cell Biol*. 1997;139(2):375–385.
41. Hamer PW, McGeachie JM, Davies MJ, Grounds MD. Evans Blue Dye as an in vivo marker of myofibre damage: optimising parameters for detecting initial myofibre membrane permeability. *J Anat*. 2002;200(pt 1):69–79.
42. Coulton GR MJ. The mdx mouse skeletal muscle myopathy: I. A histological, morphometric and biochemical investigation. *Neuropathol Appl Neurobiol*. 1988;14(1):53–70.
43. Brazeau GA, Mathew M, Entrikin RK. Serum and organ indices of the mdx dystrophic mouse. *Res Commun Chem Pathol Pharmacol*. 1992;77(2):179–189.
44. McMillan HJ, Gregas M, Darras BT, Kang PB. Serum transaminase levels in boys with Duchenne and Becker muscular dystrophy. *Pediatrics*. 2011; 127(1):e132–e136.
45. Kobayashi YM, et al. Sarcolemma-localized nNOS is required to maintain activity after mild exercise. *Nature*. 2008;456(7221):511–515.
46. Kobayashi YM, Rader EP, Crawford RW, Campbell KP. Endpoint measures in the mdx mouse relevant for muscular dystrophy pre-clinical studies. *Neuromuscular Disorders*. 2012;22(1):34–42.
47. Lynch GS, Hinkle RT, Chamberlain JS, Brooks SV, Faulkner JA. Force and power output of fast and slow skeletal muscles from mdx mice 6–28 months old. *J Physiol*. 2001;535(pt 2):591–600.
48. Webster C, Silberstein L, Hays AP, Blau HM. Fast muscle fibers are preferentially affected in Duchenne muscular dystrophy. *Cell*. 1988;52(4):503–513.
49. Dorchies OM, et al. The anticancer drug Tamoxifen counteracts the pathology in a mouse model of duchenne muscular dystrophy. *Am J Pathol*. 2013; 182(2):485–504.
50. Bloemberg D, Quadrilatero J. Rapid determination of myosin heavy chain expression in rat, mouse, and human skeletal muscle using multicolor immunofluorescence analysis. *PLoS One*. 2012; 7(4):e35273.
51. Pallafacchina G, Calabria E, Serrano AL, Kalhovde JM, Schiaffino S. A protein kinase B-dependent and rapamycin-sensitive pathway controls skeletal muscle growth but not fiber type specification. *Proc Natl Acad Sci U S A*. 2002;99(14):9213–9218.
52. Wijesekara N, et al. Muscle-specific Pten deletion protects against insulin resistance and diabetes. *Mol Cell Biol*. 2005;25(3):1135–1145.
53. Blaauw B, et al. Inducible activation of Akt increases skeletal muscle mass and force without satellite cell activation. *FASEB J*. 2009;23(11):3896–3905.
54. Wineinger MA, Abresch RT, Walsh SA, Carter GT. Effects of aging and voluntary exercise on the function of dystrophic muscle from mdx mice. *Am J Phys Med Rehabil*. 1998;77(1):20–27.
55. Xu J, Li R, Workeneh B, Dong Y, Wang X, Hu Z. Transcription factor FoxO1, the dominant mediator of muscle wasting in chronic kidney disease, is inhibited by microRNA-486. *Kidney Int*. 2012; 82(4):401–411.
56. Chen Y-W, Zhao P, Borup R, Hoffman EP. Expression profiling in the muscular dystrophies: identification of novel aspects of molecular pathophysiology. *J Cell Biol*. 2000;151(6):1321–1336.
57. Couteaux R, Mira J-C, d'Albis A. Regeneration of muscles after cardiotoxin injury I. Cytological aspects. *Biol Cell*. 1988;62(2):171–182.
58. Bishop A, Gallup B, Skeate Y, Dubowitz V. Morphological studies on normal and diseased human muscle in culture. *J Neurol Sci*. 1971;13(3):333–350.
59. Blau HM, Webster C, Pavlath GK. Defective myoblasts identified in Duchenne muscular dystrophy. *Proc Natl Acad Sci U S A*. 1983;80(15):4856–4860.
60. Sandri M, et al. Caspase 3 expression correlates with skeletal muscle apoptosis in Duchenne and facioscapulo human muscular dystrophy. A potential target for pharmacological treatment? *J Neuropathol Exp Neurol*. 2001;60(3):302–312.
61. Tews DS. Characterization of initiator and effector caspase expressions in dystrophinopathies. *Neuropathology*. 2006;26(1):24–31.
62. Sanz-Moreno V, et al. Rac activation and inactivation control plasticity of tumor cell movement. *Cell*. 2008;135(3):510–523.
63. Yang W-H, et al. RAC1 activation mediates Twist1-induced cancer cell migration. *Nat Cell Biol*. 2012; 14(4):366–374.
64. Tachi N, Hashimoto Y, Matsuoka M. MOCA is an integrator of the neuronal death signals that are activated by familial Alzheimer's disease-related mutants of amyloid β precursor protein and presenilins. *Biochem J*. 2012;442(2):413–422.
65. Fujio Y, Guo K, Mano T, Mitsuuchi Y, Testa JR, Walsh K. Cell cycle withdrawal promotes myogenic induction of Akt, a positive modulator of myocyte survival. *Mol Cell Biol*. 1999;19(7):5073–5082.
66. Namekata K, Enokido Y, Iwasawa K, Kimura H. MOCA induces membrane spreading by activating Rac1. *J Biol Chem*. 2004;279(14):14331–14337.
67. Genot EM, Arrieumerlou C, Ku G, Burgering BMT, Weiss A, Kramer IM. The T-cell receptor regulates Akt (protein kinase B) via a pathway involving Rac1 and phosphatidylinositide 3-kinase. *Mol Cell Biol*. 2000;20(15):5469–5478.
68. Oak SA, Zhou YW, Jarrett HW. Skeletal muscle

signaling pathway through the dystrophin glycoprotein complex and Rac1. *J Biol Chem*. 2003; 278(41):39287–39295.
69. Zhou YW, Thomason DB, Gullberg D, Jarrett HW. Binding of laminin α1-chain LG4-5 domain to α-dystroglycan causes tyrosine phosphorylation of syntrophin to initiate Rac1 signaling. *Biochemistry*. 2006;45(7):2042–2052.
70. Chockalingam PS, Cholera R, Oak SA, Zheng Y, Jarrett HW, Thomason DB. Dystrophin-glycoprotein complex and Ras and Rho GTPase signaling are altered in muscle atrophy. *Am J Physiol Cell Physiol*. 2002;283(2):C500–C511.
71. Vasyutina E, Martarelli B, Brakebusch C, Wende H, Birchmeier C. The small G-proteins Rac1 and Cdc42 are essential for myoblast fusion in the mouse. *Proc Natl Acad Sci U S A*. 2009;106(22):8935–8940.
72. Hochreiter-Hufford AE, et al. Phosphatidylserine receptor BAI1 and apoptotic cells as new promoters of myoblast fusion. *Nature*. 2013;497(7448):263–267.
73. Song MS, Salmena L, Pandolfi PP. The functions and regulation of the PTEN tumour suppressor. *Nat Rev Mol Cell Biol*. 2012;13(5):283–296.
74. Sanchez-Gurmaches J, Hung C-M, Tang Y, Li H. PTEN loss in the Myf5 lineage redistributes body fat and reveals subsets of white adipocytes that arise from Myf5 precursors. *Cell Metab*. 2012; 16(3):348–362.
75. Pal A, et al. PTEN mutations as a cause of constitutive insulin sensitivity and obesity. *N Engl J Med*. 2012;367(11):1002–1011.
76. Namekata K, et al. Dock3 attenuates neural cell death due to NMDA neurotoxicity and oxidative stress in a mouse model of normal tension glaucoma. *Cell Death Differ*. 2013;20(9):1250–1256.
77. de Silva MG, et al. Disruption of a novel member of a sodium/hydrogen exchanger family and DOCK3 is associated with an attention deficit hyperactivity disorder-like phenotype. *J Med Genet*. 2003; 40(10):733–740.
78. Chen Q, Peto CA, Shelton GD, Mizisin A, Sawchenko PE, Schubert D. Loss of modifier of cell adhesion reveals a pathway leading to axonal degeneration. *J Neurosci*. 2009;29(1):118–130.
79. Charrasse S, Comunale F, Grumbach Y, Poulat F, Blangy A, Gauthier-Rouvière C. RhoA GTPase regulates M-cadherin activity and myoblast fusion. *Mol Biol Cell*. 2006;17(2):749–759.
80. Charrasse S, Comunale F, Fortier M, Portales-Casamar E, Debant A, Gauthier-Rouvière C. M-cadherin activates Rac1 GTPase through the Rho-GEF trio during myoblast fusion. *Mol Biol Cell*. 2007;18(5):1734–1743.
81. Côté J-F, Vuori K. Identification of an evolutionarily conserved superfamily of DOCK180-related proteins with guanine nucleotide exchange activity. *J Cell Sci*. 2002;115(pt 24):4901–4913.
82. Samson T, et al. Def-6, a guanine nucleotide exchange factor for Rac1, interacts with the skeletal muscle integrin chain α7A and influences myoblast differentiation. *J Biol Chem*. 2007;282(21):15730–15742.
83. Matsuda C, et al. Affixin activates Rac1 via βPIX in C2C12 myoblast. *FEBS Lett*. 2008;582(8):1189–1196.
84. Jungmichel S, Sylvestersen KB, Choudhary C, Nguyen S, Mann M, Nielsen ML. Specificity and commonality of the phosphoinositide-binding proteome analyzed by quantitative mass spectrometry. *Cell Rep*. 2014;6(3):578–591.
85. Cacchiarelli D, et al. MicroRNAs involved in molecular circuitries relevant for the Duchenne muscular dystrophy pathogenesis are controlled by the dystrophin/nNOS pathway. *Cell Metab*. 2010; 12(4):341–351.
86. Alexander MS, et al. MicroRNA-199a is induced in dystrophic muscle and affects WNT signaling, cell proliferation, and myogenic differentiation. *Cell Death Differ*. 2013;20(9):1194–1208.
87. Roberts TC, et al. Expression analysis in multiple muscle groups and serum reveals complexity in the microRNA transcriptome of the mdx mouse with implications for therapy. *Mol Ther Nucleic Acids*. 2012;1:e39.
88. Poliseno L, Salmena L, Zhang J, Carver B, Haveman WJ, Pandolfi PP. A coding-independent function of gene and pseudogene mRNAs regulates tumour biology. *Nature*. 2010;465(7301):1033–1038.
89. Tay Y, et al. Coding-independent regulation of the tumor suppressor PTEN by competing endogenous mRNAs. *Cell*. 2011;147(2):344–357.
90. van Rooij E, et al. A family of microRNAs encoded by myosin genes governs myosin expression and muscle performance. *Dev Cell*. 2009;17(5):662–673.
91. Chen J-F, et al. microRNA-1 and microRNA-206 regulate skeletal muscle satellite cell proliferation and differentiation by repressing Pax7. *J Cell Biol*. 2010; 190(5):867–879.
92. Goljanek-Whysall K, Pais H, Rathjen T, Sweetman D, Dalmay T, Münsterberg A. Regulation of multiple target genes by miR-1 and miR-206 is pivotal for C2C12 myoblast differentiation. *J Cell Sci*. 2012; 125(pt 15):3590–3600.
93. Zhao Y, Samal E, Srivastava D. Serum response factor regulates a muscle-specific microRNA that targets Hand2 during cardiogenesis. *Nature*. 2005; 436(7048):214–220.
94. Chen J-F, et al. The role of microRNA-1 and microRNA-133 in skeletal muscle proliferation and differentiation. *Nat Genet*. 2006;38(2):228–233.
95. McCarthy JJ, Esser KA, Andrade FH. MicroRNA-206 is overexpressed in the diaphragm but not the hindlimb muscle of mdx mouse. *Am J Physiol Cell Physiol*. 2007;293(1):C451–C457.
96. Liu N, et al. Mice lacking microRNA 133a develop dynamin 2-dependent centronuclear myopathy. *J Clin Invest*. 2011;121(8):3258–3268.
97. Bitoun M, et al. Mutations in dynamin 2 cause dominant centronuclear myopathy. *Nat Genet*. 2005; 37(11):1207–1209.
98. Wang L, et al. Loss of miR-29 in myoblasts contributes to dystrophic muscle pathogenesis. *Mol Ther*. 2012;20(6):1222–1233.
99. Liu N, et al. microRNA-206 promotes skeletal muscle regeneration and delays progression of Duchenne muscular dystrophy in mice. *J Clin Invest*. 2012; 122(6):2054–2065.
100. Hitachi K, Nakatani M, Tsuchida K. Myostatin signaling regulates Akt activity via the regulation of miR-486 expression. *Int J Biochem Cell Biol*. 2014; 47:93–103.
101. Miyazaki Y, et al. Viral delivery of miR-196a ameliorates the SBMA phenotype via the silencing of CELF2. *Nat Med*. 2012;18(7):1136–1141.
102. Quattrocelli M, et al. Long-term miR-669a therapy alleviates chronic dilated cardiomyopathy in dystrophic mice. *J Am Heart Assoc*. 2013;2(4):e000284.
103. Mendell JR, et al. Dystrophin immunity in Duchenne's muscular dystrophy. *N Engl J Med*. 2010; 363(15):1429–1437.
104. Shin J-H, Hakim CH, Zhang K, Duan D. Genotyping mdx, mdx3cv, and mdx4cv mice by primer competition polymerase chain reaction. *Muscle Nerve*. 2011; 43(2):283–286.
105. Choi SJ, Widrick JJ. Combined effects of fatigue and eccentric damage on muscle power. *J Appl Physiol (1985)*. 2009;107(4):1156–1164.
106. Widrick JJ, Jiang S, Choi SJ, Knuth ST, Morcos PA. An octaguanidine–morpholino oligo conjugate improves muscle function of mdx mice. *Muscle Nerve*. 2011;44(4):563–570.
107. Livak KJ, Schmittgen TD. Analysis of relative gene expression data using real-time quantitative PCR and the 2(-Delta Delta C(T)) Method. *Methods*. 2001; 25(4):402–408.